OXFORD

Cerebral Cortex, February 2020;30: 730–752

doi: 10.1093/cercor/bhz122
Advance Access Publication Date: 2 July 2019
Feature Article

FEATURE ARTICLE

Differential Structure of Hippocampal CA1 Pyramidal Neurons in the Human and Mouse

Ruth Benavides-Piccione[1,2,*], Mamen Regalado-Reyes[2], Isabel Fernaud-Espinosa[2], Asta Kastanauskaite[2], Silvia Tapia-González[2], Gonzalo León-Espinosa[2,3], Concepcion Rojo[4], Ricardo Insausti[5], Idan Segev[6,7] and Javier DeFelipe[1,2]

[1]Instituto Cajal, Consejo Superior de Investigaciones Científicas (CSIC), Madrid 28002, Spain, [2]Laboratorio Cajal de Circuitos Corticales, Centro de Tecnología Biomédica, Universidad Politécnica de Madrid, Madrid 28223, Spain, [3]Departamento de Química y Bioquímica, Facultad de Farmacia, Universidad San Pablo Centro de Estudios Universitarios (CEU), Madrid 28925, Spain, [4]Sección Departamental de Anatomía y Embriología (veterinaria). Facultad de Veterinaria. Universidad Complutense de Madrid 28040, Spain, [5]Laboratorio de Neuroanatomía Humana, Facultad de Medicina, Universidad de Castilla-La Mancha, Albacete 02008, Spain, [6]Department of Neurobiology, Hebrew University of Jerusalem, Jerusalem 9190501, Israel and [7]Edmond and Lily Safra Center for Brain Sciences, Hebrew University of Jerusalem, Jerusalem 9190501, Israel

Address correspondence to Ruth Benavides-Piccione, Laboratorio Cajal de Circuitos Corticales, Centro de Tecnologia Biomédica, Universidad Politécnica de Madrid, Campus Montegancedo S/N Pozuelo de Alarcón 28223, Madrid and Instituto Cajal, Consejo Superior Investigaciones Científicas (CSIC) Avenida Doctor Arce 37, Madrid 28002, Spain. Email: rbp@cajal.csic.es

Abstract

Pyramidal neurons are the most common cell type and are considered the main output neuron in most mammalian forebrain structures. In terms of function, differences in the structure of the dendrites of these neurons appear to be crucial in determining how neurons integrate information. To further shed light on the structure of the human pyramidal neurons we investigated the geometry of pyramidal cells in the human and mouse CA1 region—one of the most evolutionary conserved archicortical regions, which is critically involved in the formation, consolidation, and retrieval of memory. We aimed to assess to what extent neurons corresponding to a homologous region in different species have parallel morphologies. Over 100 intracellularly injected and 3D-reconstructed cells across both species revealed that dendritic and axonal morphologies of human cells are not only larger but also have structural differences, when compared to mouse. The results show that human CA1 pyramidal cells are not a stretched version of mouse CA1 cells. These results indicate that there are some morphological parameters of the pyramidal cells that are conserved, whereas others are species-specific.

Key words: comparative neuroanatomy, dendrites, hippocampal formation, intracellular injections, principal neurons, 3D reconstructions

Introduction

Pyramidal neurons are the most common cell type and the main projection neurons in the cerebral cortex (neocortex and allocortex). Therefore, most of the information processed in a given cortical region is transferred through the pyramidal cell axons to other cortical or subcortical regions. The dendritic spines of pyramidal cells are the main postsynaptic target of excitatory glutamatergic synapses. In turn, pyramidal cell axons constitute the main source of these synapses in both the neocortex and the hippocampal formation (reviewed in DeFelipe and Fariñas 1992; Anderson et al. 2007; Cenquizca and Swanson 2007). In general, the dendritic structure of these neurons can be described as follows (DeFelipe and Fariñas 1992): from the upper pole of the cell body arises a prominent apical dendrite directed radially toward the pia mater, giving off a number of oblique collaterals that usually terminate in an apical tuft. From the base of the soma, several laterally or downward-directed dendrites emerge forming the basal arbor. The axon also emerges from the base of the cell or from the origin of a basal dendrite; this axon is directed downwards and may give off several collaterals. There are large variations in the pyramidal cell structure depending on the layer, cortical region, and species where the pyramidal cell is located. For example, pyramidal cells in the associative temporal and prefrontal lobe of primates exhibit greater dendritic complexity than those in other sensory areas (Elston et al. 2001; Jacobs et al. 2001; Bianchi et al. 2013). Rodents also show regional and layer variations in pyramidal cell structure, although these variations are much less pronounced than in humans (Benavides-Piccione et al. 2002; Benavides-Piccione et al. 2006; Ballesteros-Yáñez et al. 2010; Mohan et al. 2015; van Aerde and Feldmeyer 2015; Rojo et al. 2016; Deitcher et al. 2017). Furthermore, a number of studies have shown differences in morphology and intrinsic electrophysiological characteristics of pyramidal cells located at depth versus superficially in the pyramidal cell layer of the CA1 region of the hippocampus (Bannister and Larkman 1995; Jarsky et al. 2008; Lee et al. 2014; Valero and de la Prida 2018). Since the dendritic tree structure influences the biophysical and computational properties of neurons, differences in pyramidal cell structure are not only important determinants of variations of the functional organization of the cerebral cortex (reviewed in Stuart and Spruston 2015) but are also highly relevant from the evolutionary point of view (DeFelipe 2011).

Nevertheless, a constraint on comparing neurons in human versus other species is the question of the homology of the areas between species. One of the most evolutionary conserved archicortical region is the hippocampus (e.g., Stephan and Andy 1970), a brain structure critically involved in the formation, consolidation, and retrieval of memory. However, no detailed morphological studies of human CA1 pyramidal cells are available. Thus, to further shed light on the structure of human pyramidal neurons and possible differences between species, in the present study we investigated the geometry of pyramidal cells in the CA1 region of the human and mouse hippocampus. Furthermore, CA1 is of particular interest since, during the course of evolution, it is clear that the human pyramidal cell layer became much less densely packed than that of the mouse (Fig. 1). This process may not be due to a brain size scaling effect since, for example, the extent of the pyramidal cell layer in the CA1 region of the elephant or the giraffe (which have larger brains) is smaller than that of the human (Defelipe's laboratory unpublished observations; see also Slomianka et al. 2011 and Patzke et al. 2013). This process, sometimes called "corticalization" of the human CA1 pyramidal cell layer because it resembles a neocortical cytoarchitecture, most probably has fundamental functional and hodological consequences: The basal and apical dendrites of human pyramidal cells are intermixed in the pyramidal cell layer, whereas in the mouse the basal and apical dendritic domains are basically separated (basal dendrites in the stratum oriens; apical dendrites in the stratum radiatum). In the present study, over 100 intracellularly injected cells that were 3D-reconstructed from confocal microscopy images were examined. The main finding is that CA1 pyramidal neurons show characteristic cell morphology. Human cells are not only larger but also have a different structural organization compared to mouse pyramidal cells for particular morphological features. However, there are some other morphological variables that, despite differing in their absolute values, show similar patterns of distribution between the two species. The possible implications of these structural differences between human and mouse are elaborated in the "Discussion".

Materials and Methods

Tissue Preparation

Human brain tissue was obtained at autopsy from the Unidad Asociada Neuromax—Laboratorio de Neuroanatomía Humana, Facultad de Medicina, Universidad de Castilla-La Mancha, Albacete, Spain, and Laboratorio Cajal de Circuitos Corticales Universidad Politécnica de Madrid-Consejo Superior de Investigaciones Científicas (CSIC), Madrid, Spain. The tissue was obtained following national laws and international ethical and technical guidelines on the use of human samples for biomedical research purposes. In this study, we used coronal sections of the human hippocampus at the level of the hippocampal body (Insausti and Amaral 2012) of two cases obtained within a postmortem interval of 2–3 h; one male (AB1) aged 45 and one female (AB2) aged 53. These cases were used as controls in a previous study unrelated to the present investigation (Domínguez-Álvaro et al. 2018). Upon removal, the brains were immersed in cold 4% paraformaldehyde in 0.1 M phosphate buffer (PB), pH 7.4, and sectioned into thick coronal slabs to facilitate fixation. Small blocks from the hippocampal formation were then extracted and transferred to a second solution of 4% paraformaldehyde in PB for 24 h at 4 °C. Then, vibratome sections (300 µm) of the CA1 region were obtained in the coronal plane.

Mouse tissue samples were obtained from C57BL/6 adult (8-week-old) male mice ($n = 9$; id6, id7, id8, id10, id14, id15, id20, id21, and id68). All animals were overdosed by intraperitoneal injection of sodium pentobarbitone and were perfused via the heart with phosphate-buffered saline (0.1 M PBS) followed by 4% paraformaldehyde in PB. Their brains were then removed and further immersed in 4% paraformaldehyde for 24 h. Coronal sections (200 µm) were obtained with a vibratome, which included the dorsal CA1 region (Paxinos and Franklin 2004).

Intracellular Injections and Immunocytochemistry

Human and mouse sections were prelabeled with 4′,6-diamidino-2-phenylindole (DAPI; Sigma, St Louis, MO), and a continuous

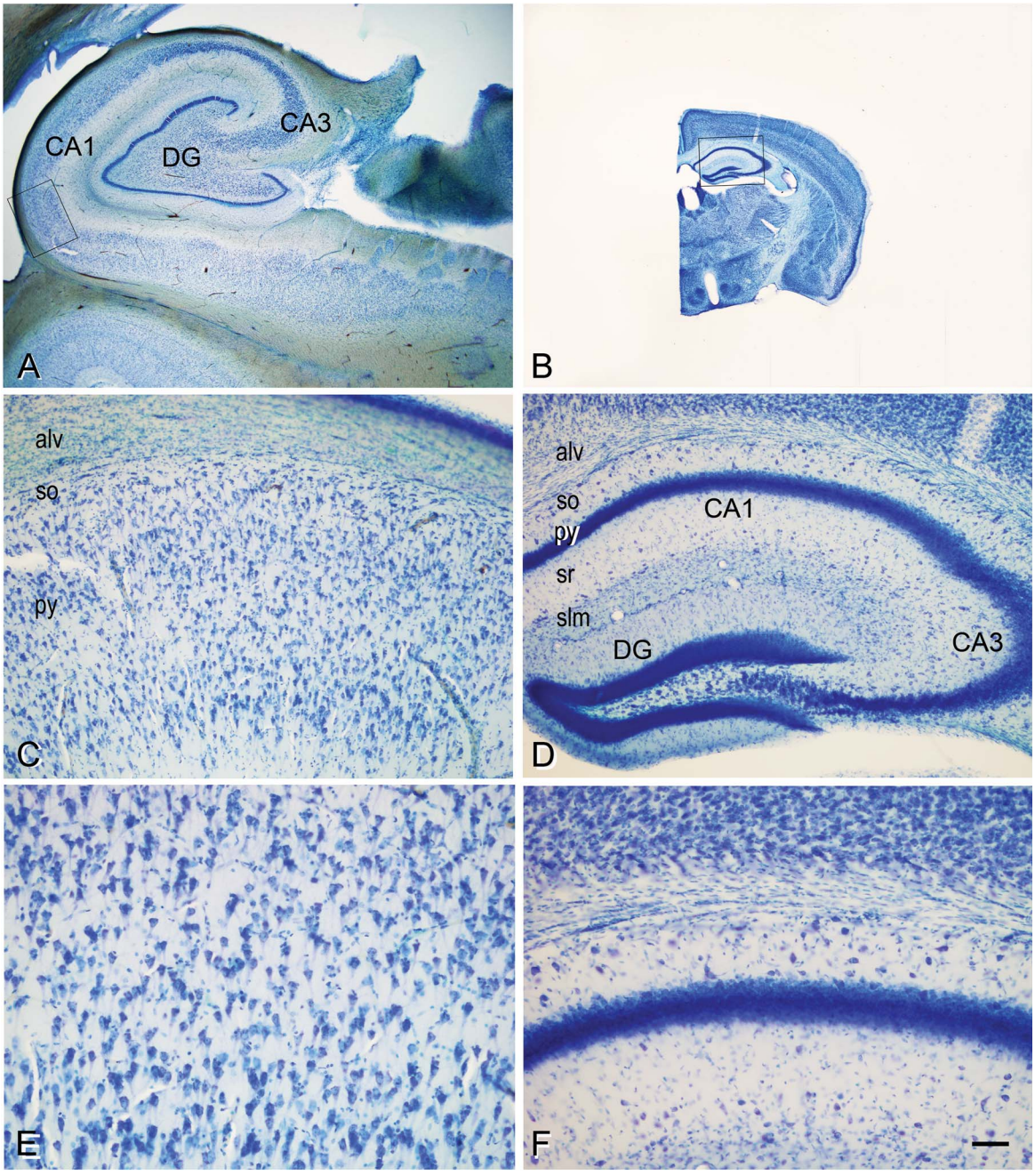

Figure 1. (*A* and *B*) Low-power photomicrographs of Nissl-stained coronal brain sections from human (*A*) and mouse (*B*) at the same magnification to illustrate differences in brain size. (*C* and *D*) Higher magnification images of boxed areas shown in (*A*) and (*B*) showing the CA1 hippocampal field of the human (*C*) and mouse (*D*) at the same magnification, respectively. (*E* and *F*) Higher magnification photomicrographs from CA1 human (*E*) and mouse (*F*) pyramidal cell layer shown in (*C*) and (*D*), respectively, to illustrate differences in the arrangement of cells. Scale bar (in panel F) is equal to 1000 µm in (*A*) and (*B*); 120 µm in (*C*) and (*D*); 60 µm in (*E*) and (*F*). alv means alveus; so, stratum oriens; py, stratum pyramidale; sr, stratum radiatum; slm, stratum lacunosum moleculare.

current was used to inject individual cells with Lucifer yellow (LY; 8% in 0.1M Tris buffer, pH 7.4) in the pyramidal cell layer of the CA1 field of the human (Fig. 2) and mouse (Fig. 3) hippocampus. We did not distinguish between superficial and deep CA1 pyramidal cells. However, we injected approximately in the middle of the CA1 pyramidal cell layer of the dorsal hippocampus in the mouse and at the level of the hippocampal body in the human. Regarding regional limits we specifically avoided CA1/CA2 and CA1/subiculum border cells. LY was applied to each injected cell by continuous current until the distal tips of each cell fluoresced brightly, indicating that the dendrites were completely filled and ensuring that the fluorescence did not diminish at a distance from the soma. Following the intracellular injections, the sections were immunostained for LY using rabbit antisera against LY (1:400 000; generated at the Cajal Institute) diluted in stock solution (2% bovine serum albumin, 1% Triton

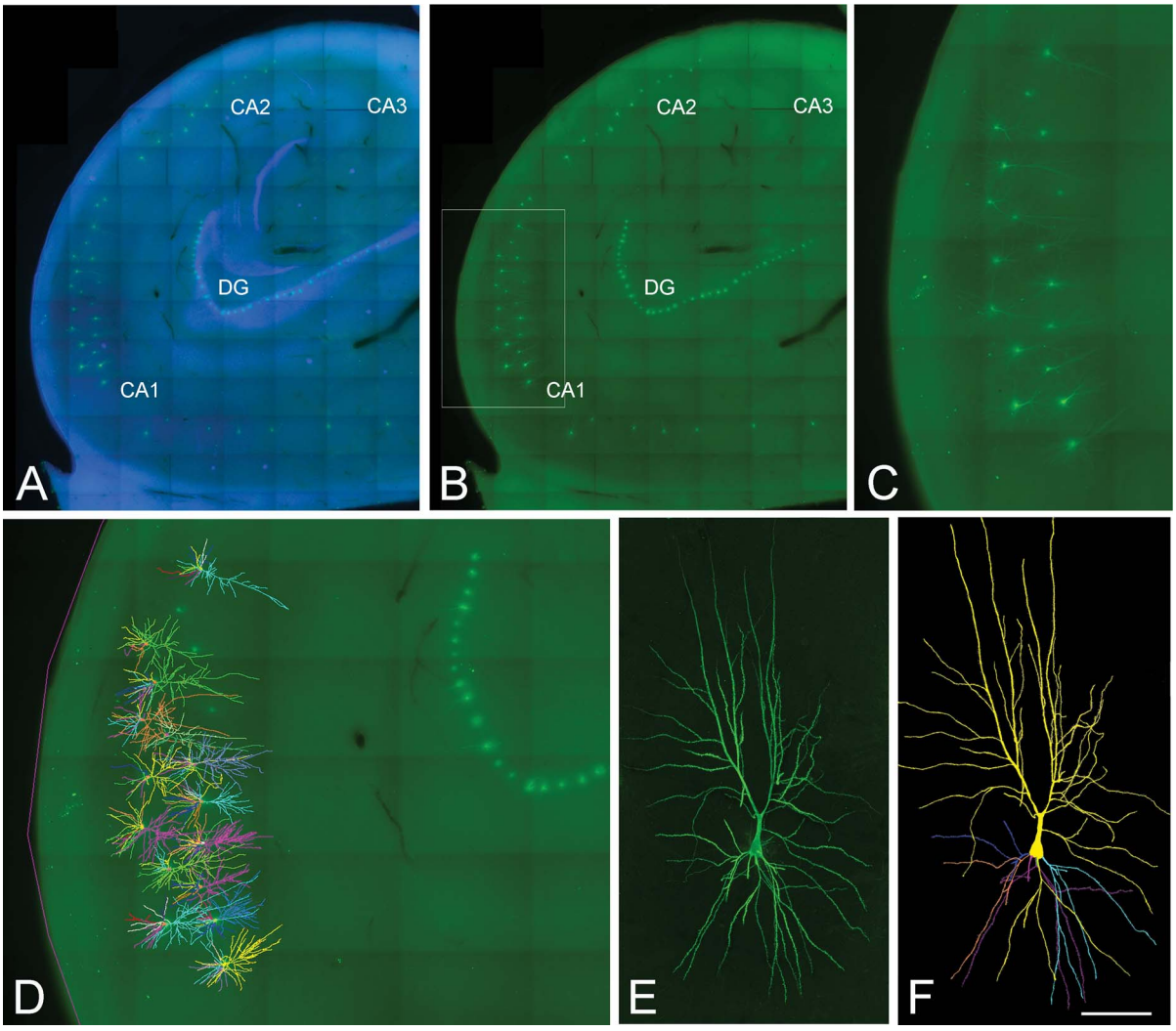

Figure 2. Confocal microscopy images of human neurons injected with LY in the hippocampus. (*A* and *B*) Labeled pyramidal cells (green) and DAPI staining (blue) in different regions of the human hippocampus, including CA1, CA2, CA3, and the dentate gyrus (DG) region. (*C*) Higher magnification image of the boxed region shown in (*B*). (*D*) 3D-reconstructed cells superimposed on the confocal image shown in (*C*). (*E* and *F*) High-magnification image z projection showing an injected CA1 pyramidal cell (*E*) and the 3D reconstruction of the same cell (*F*). Scale bar (in panel F) is equal to 1100 µm in (*A*) and (*B*); 460 µm in (*C*) and (*D*); 100 µm in (*E*) and (*F*).

X-100, and 5% sucrose in PB). The sections were then incubated in biotinylated donkey anti-rabbit IgG (1:100; Amersham, Buckinghamshire, UK) and streptavidin-conjugated Alexa fluor 488 (1:1000; Molecular Probes, Eugene, OR, USA). Finally, the sections were washed and mounted with ProLong Gold Antifade Reagent (Invitrogen Corporation, Carlsbad, CA, USA). See Elston et al. (2001) and Benavides-Piccione et al. (2013) for further details of the cell injection methodology.

Cell Reconstruction and Quantitative Analysis

Sections were imaged with a Leica TCS 4D confocal scanning laser attached to a Leitz DMIRB fluorescence microscope. Fluorescent labeling profiles were imaged, using an excitation wavelength of 491 nm to visualize Alexa fluor 488. Consecutive stacks of images at high magnification (×63 glycerol; voxel size, $0.240 \times 0.240 \times 0.29$ µm^3 for human cells and $0.120 \times 0.120 \times 0.13$ µm^3 for mouse cells) were acquired to capture dendrites along the apical and basal dendritic arbors. Since intracellular injections of the pyramidal cell were performed in 200- and 300-µm-thick coronal sections, the part of the dendritic arbor nearest the surface of the slice from which the cell soma was injected (typically at a depth of ~30 µm from the surface) was lost. The slices were of sufficient thickness in each species so as to include all dendrites that run toward the depth of the slice. Using a similar method of intracellular injection, Krimer et al. (1997) estimated that the reconstruction of neurons represented approximately two-thirds of the total dendritic arbor of pyramidal cells. Nonetheless, it is important to mention that the percentage of the basal arbor and apical arbor included within the section may vary in each cell, depending on how parallel the main apical dendrite runs with respect to the surface of the slice. In the present study, neurons were included in the analysis if they showed a main apical dendrite of at least 200 µm in length in both human and mouse cells. Furthermore, dendrites that ran for further than ~ 900 µm from the soma were not properly filled with dye, and therefore distal apical dendrites (apical tufts) of human cells were not included in the analysis.

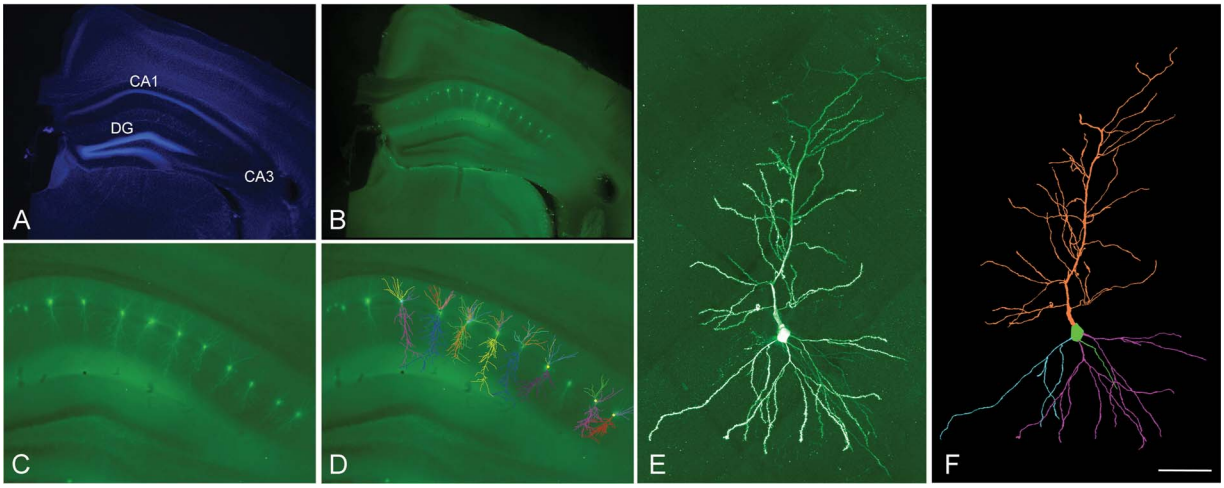

Figure 3. Confocal microscopy images of mouse neurons injected with LY in the hippocampus. (*A*) DAPI staining. (*B*) Labeled pyramidal cells in the CA1 hippocampal field. (*C*) Higher magnification photomicrographs of the image shown in (*B*). (*D*) 3D-reconstructed cells superimposed on the confocal image shown in (*C*). (*E* and *F*) High-magnification image z projection showing an injected CA1 pyramidal cell (*E*) and the 3D reconstruction of the same cell (*F*). Scale bar (in panel F) is equal to 750 µm in (*A*) and (*B*); 300 µm in (*C*) and (*D*); 50 µm in (*E*) and (*F*).

The following numbers of cells were sampled from each case: human AB1 (31 cells) and AB2 (23 cells), and mouse id6 (4 cells), id7 (9 cells), id8 (3 cells), id10 (6 cells), id14 (10 cells), id15 (2 cells), id20 (7 cells), id21 (4 cells), and id68 (5 cells).

Data points of neuron morphology of each pyramidal cell included in the analysis (54 human cells and 50 mouse cells; Fig. 4) were extracted in 3D using Neurolucida 360 (MicroBrightfield, VT, USA). Briefly, the apical and basal dendrites, as well as the axon and soma, were reconstructed through manually traced 3D points, delimiting the different segments that form the cell arbor. These points have an associated diameter that automatically provides the information of the varying thickness of the dendrite at that particular point and varies along the length of the dendrite. Axons were only traced if they were included within the section over a length of at least 50 µm. The soma was defined through a set of connected points tracing the contour of the soma in 2D. The cells were traced by three experts, and two additional experts re-examined the reconstructions searching for possible mistakes.

Several morphological variables were extracted using Neurolucida software. Some of the features measured did not depend on the entirety of the reconstructed cell and can thus be considered as full measurements: mean soma area (estimated by measuring the area of the maximum perimeter of the soma); dendritic/axonal average segment diameter, segment length, segment surface area, and segment volume; as well as axonal varicosity density (defined as a swelling of the axon exceeding the typical variation in diameter of the adjacent axonal shafts per axonal length) and intervaricosity distance (defined as distance between two adjacent axonal varicosities). However, other morphological variables did depend on the entirety of the cell, and, thus, may only partially describe the cell and can be considered "non-full" measurements: area and volume of the dendritic arbor (2D and 3D convex hulls), total number of dendrites, total number of nodes, total dendritic length, total dendritic surface area, and total dendritic volume.

Values are expressed as total numbers, per branch order segment and as a function of the distance from soma (Sholl analysis). Only dendritic segments that were completely reconstructed were included in the analysis. All statistical analyses were performed using GraphPad Prism version 5.00 for Windows (GraphPad Software, San Diego, CA, USA). When morphological parameters were presented as mean values, the Kruskal–Wallis test was used to compare between the groups. The reported *P*-values were corrected for multiple testing with Dunn's post-test. Measurements reported as a function of the distance from the soma were analyzed using Friedman test. Mann–Whitney test was used for pairwise comparisons. Differences were considered to be significant when $P < 0.05$. Measurements are reported as mean ± standard error of mean (SEM), unless otherwise indicated.

Results

Human CA1 Pyramidal Cells

Fifty-four pyramidal cells were analyzed in the CA1 field of the human hippocampus. These cells presented a mean cell body area of 350 ± 9.7 µm^2.

Apical Dendrites

The apical arbor emerged from the soma of the cells and was composed of a prominent main apical dendrite, which gave off a number of oblique collaterals but the apical tufts were not labeled (see Materials and Methods section for further details). The extent of the apical dendrites ranged from 230 to 800 µm with the number of collaterals ranging from 6 to 33. The apical arbor included the thickest and longest segments, which belonged mainly to the main apical dendrite, whereas collateral dendrites showed segments that were slightly thinner and longer than basal segments (Fig. 5A–D).

The main apical dendritic shaft could be followed in all labeled neurons for at least the first 200 µm. The structure of this portion of the apical dendrite varied: Some cells had an ascending course without branching (22%), while others bifurcated once (24%), twice (30%), or three times (24%). According to these features, four main patterns of apical shaft branching were observed in human cells (Fig. 6A). The dendrogram showed that

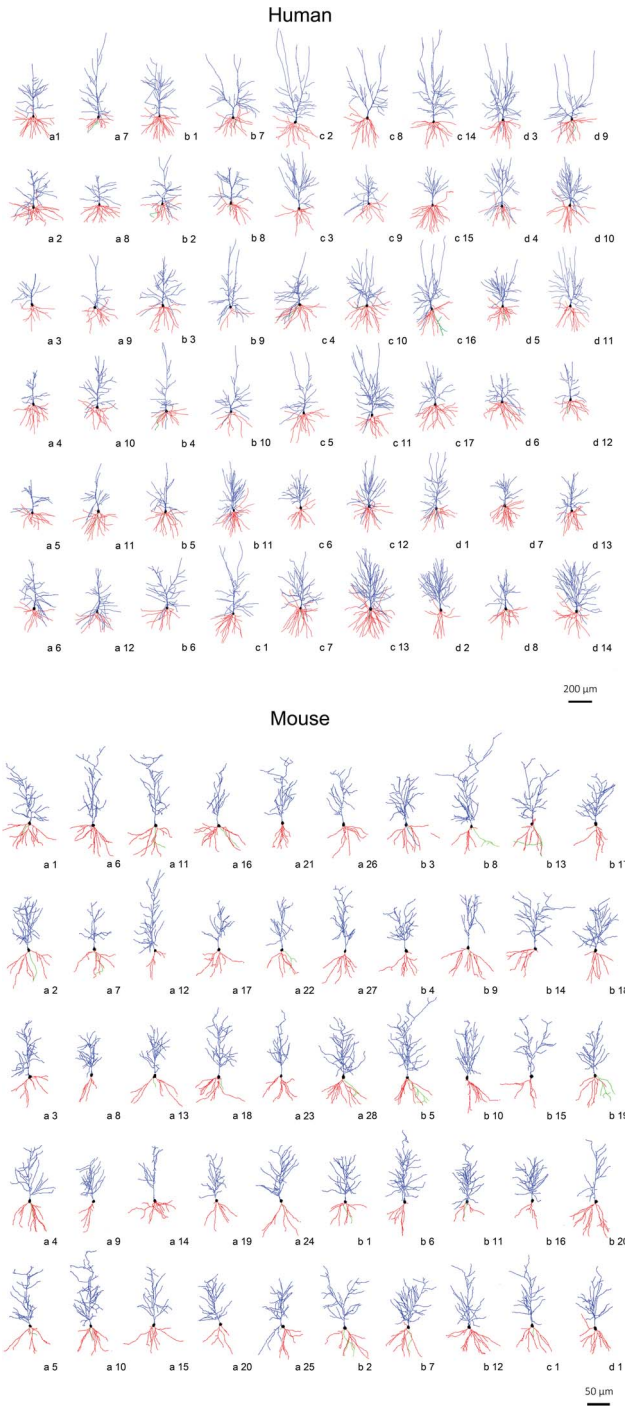

Figure 4. Drawings of the apical (blue) and basal (red) dendritic arbors of CA1 pyramidal neurons from the human and mouse. Each cell is identified with a code that indicates the type of apical branching pattern: a, 0 bifurcations; b, 1 bifurcation; c, 2 bifurcations; and d, 3 bifurcations—within the first 200 µm (see Fig. 6 and Supplementary Figs S1 and S5 for further details).

a number of these cells branched further, with the structure of the apical arbor being more complex the further away the branching occurred (Supplementary Figure S1*a–d*). The average diameter of the main apical dendrite before any bifurcation occurred was 5.74 ± 0.18 µm. When apical dendrite branching occurred, the diameter decreased as the branch order increased (Fig. 5*E*). Regarding the length of dendritic segments, they increased as branch order segment increased (only dendritic segments that were complete—and by definition excluded incomplete endings—were included in this analysis; Fig. 5*F*). However, due to large differences in diameter between dendritic orders, the surface area of the dendritic segment values per order were similar (Fig. 5*G*). Furthermore, the dendritic volume of these segments decreased toward higher orders (Fig. 5*H*).

Regarding collateral dendrites of the apical shaft, branches—as they emerged from the main apical dendrite—showed an average diameter of 1.33 ± 0.02 µm up to the first bifurcation and slightly decreased in the following branch orders (Fig. 5*E*). The mean length of the dendritic segments increased as the branch order increased (Fig. 5*F*). Similarly, surface area of the dendritic segments and their volume also increased toward higher orders (Fig. 5*G,H*). Segments were then further classified according to branching segments (meaning a segment that bifurcates) and terminal segments (meaning a segment that ends): Branching segments followed a similar pattern of diameter distribution as described above, whereas terminal segments showed similar thinner diameters regardless of their branch order (Fig. 7*A,B*). Regarding dendritic length, for both branching and terminal segments, it increased as the branch order segment increased, although terminal segments were much longer (Fig. 7*C,D*). Similarly, the surface area of both branching and terminal dendritic segments and their volume also increased toward higher orders, and terminal segments had a much larger area and volume than branching segments (Fig. 7*E–H*).

Basal Dendrites

The basal dendritic arbor showed 6.37 ± 0.25 primary branches that emerged from the soma with an average diameter of 1.98 ± 0.04 µm up to the first node and slightly decreased in diameter as the branch order segment increased (Fig. 5*E*). The mean length of the dendritic segments that composed the basal arbor increased as the branch order increased (Fig. 5*F*). Similarly, surface area of the dendritic segments and their volume also increased toward higher orders (Fig. 5*G,H*). When segments were classified according to their position within the arbor, branch segment diameter again decreased as branch order increased, while—as occurred with collateral dendrites—all segments that ended were of a similar diameter regardless of the branch order they belonged to (Fig. 7*A,B*). Regarding the length of branch segments, it increased as branch order increased, while terminal segments length decreased as branch order increased and was longer than branch segment length (Fig. 7*C,D*). Similarly, the surface area and volume of branch segments also increased toward higher orders, while terminal segments surface area and volume decreased toward higher orders and were larger than branch segments surface area and volume (Fig. 7*E,F*).

When morphological variables were measured according to their distance from the soma, it was revealed that the dendritic diameter gradually decreased as follows: from 7.19 ± 0.21 to ~1.5 µm along the first 400 µm and remaining similar at further distances in the main apical compartment (Fig. 8*A*); from 1.87 ± 0.33 to ~1 µm along the first 50 µm from the soma and then remaining similar at further distances apical collateral dendrites; and from 2.36 ± 0.20 to ~1 micron along the first

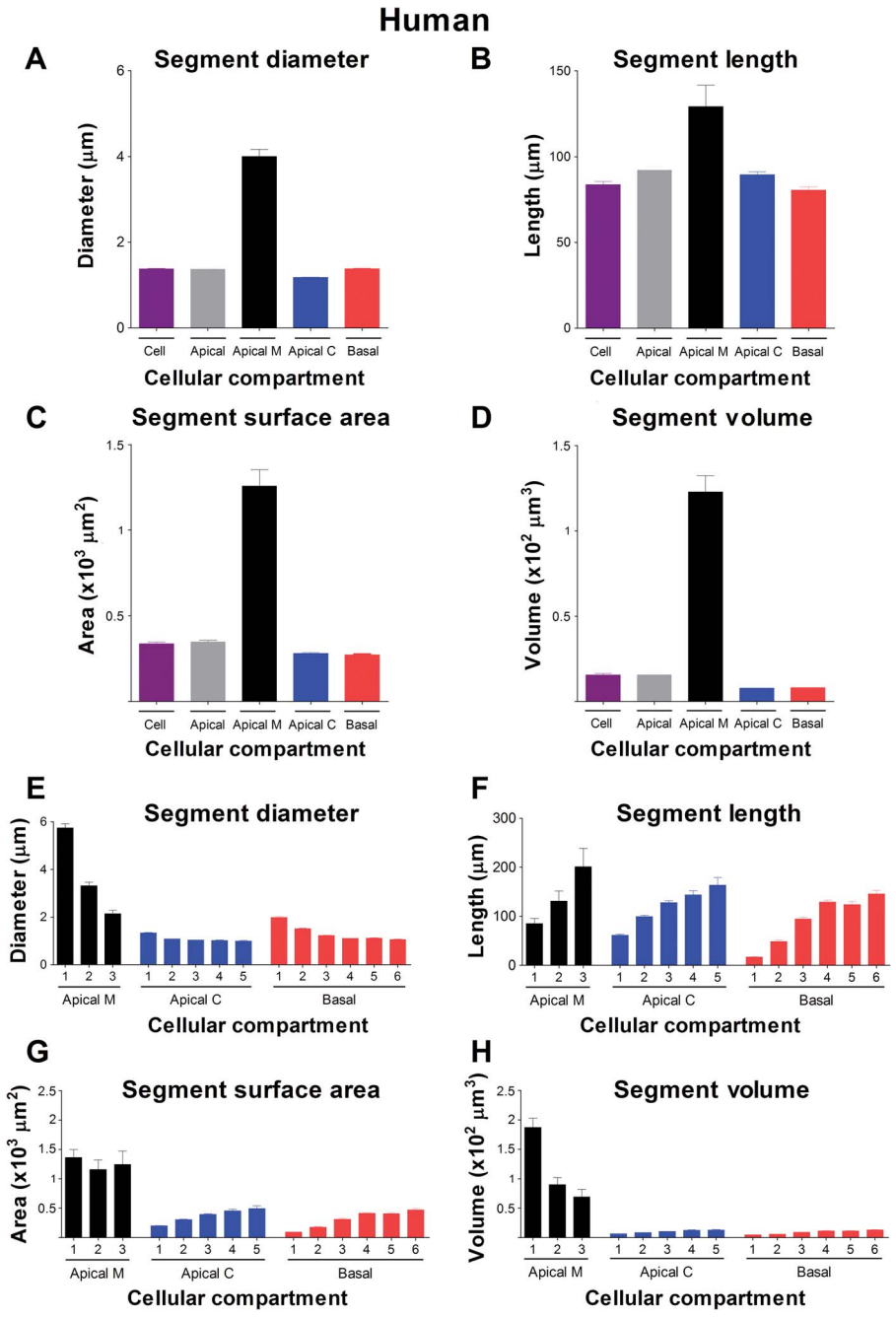

Figure 5. (*A–D*) Graphs showing human dendritic segment average diameter (*A*), segment length (*B*), segment surface area (*C*), and segment volume (*D*), expressed per cell (purple) and per dendritic compartment: apical arbor, including main apical dendrite and apical collateral dendrites together (gray); main apical dendrite alone (black); apical collateral dendrites alone (blue); and basal dendritic arbor (red). (*E–H*) Graphs showing same morphological variables as in (*A–D*): dendritic segment average diameter (*E*), segment length (*F*), segment surface area (*G*), and segment volume (*H*), expressed per branch order (1, 2, 3, etc.) and per dendritic compartment: main apical dendrite (black), apical collateral dendrites (blue), and basal arbor (red). Measurements are reported as mean ± SEM. Only dendritic segments that were complete, and thus excluding incomplete endings, were included in this analysis. Statistical significance of the differences is shown in Supplementary Tables 1 and 2.

60 µm and remaining similar at further distances in the basal dendrites (Fig. 8A).

Additional Dendritic Variables

Additional morphological variables were measured to further describe the cell, although this was limited by the partial reconstruction of the neurons. These measurements included the size of the dendritic arbor (2D and 3D convex hulls), number of nodes, number of endings, dendritic length, dendritic area, and volume expressed as total numbers and as a function of the distance from the soma (Sholl analysis) (Supplementary Figure S2 and S3). These measurements showed, for example, that the peak number of nodes in the basal arbor was located at ~40 µm and rapidly decreased (Supplementary Figure S3),

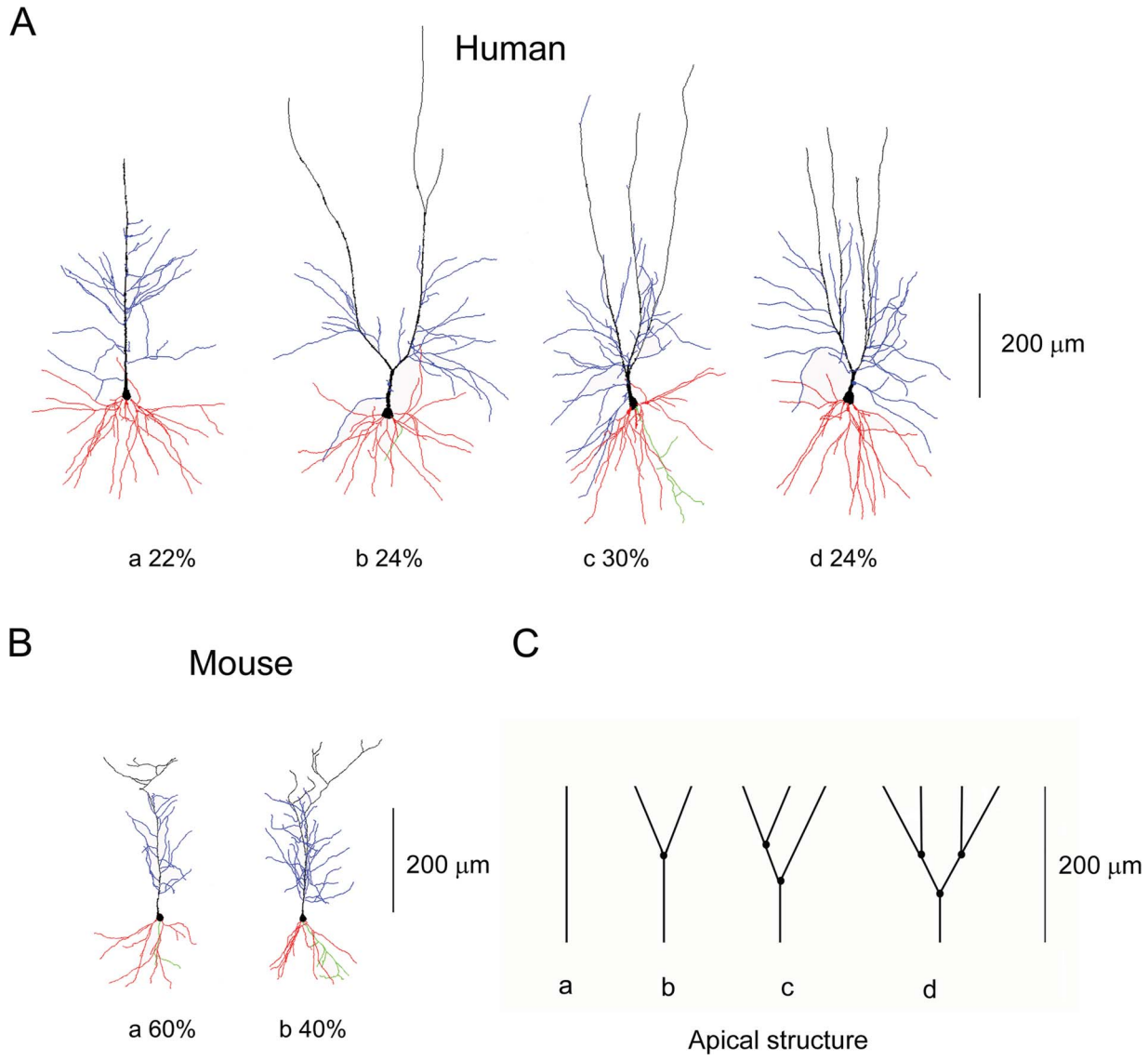

Figure 6. Representative examples of reconstructed pyramidal cells from human (*A*) and mouse (*B*) CA1 hippocampal field at the same magnification to illustrate differences in cell size. Main apical dendrite is shown in black, apical collateral dendrites in blue, and basal arbor in red. Axons (if traced) are represented in green. Note that each representative neuron in (*A*) and (*B*) includes the prevalence percentage of the corresponding pattern shown in (*C*). (*C*) Schematic representation showing different main apical branching patterns: a, 0 bifurcations; b, 1 bifurcation; c, 2 bifurcations; d, 3 bifurcations (measured within the first 200 µm).

which interestingly coincided with the location where basal dendritic diameter reached a constant value (~50 µm; Fig. 8A). However, in apical collateral dendrites, the distribution of nodes was different. The peak number of nodes was found to be located at 70 µm from the soma and progressively decreased (Supplementary Figure S3), whereas the apical collateral dendritic diameter reached a constant value at ~40 µm. Both basal and collateral dendrites showed similar distributions (Fig. 8A).

Axon

Regarding the axon, it emerged either from the soma (66%) or from the initial portion of a basal dendrite (44%). It had a mean average diameter of 3.92 ± 0.42 µm that gradually decreased to reach ~0.9 µm at a distance of ~70 µm from the soma and for the remaining distances (Fig. 8A). In the case that the axon emerged from the dendrite, its diameter was thinner (1.88 ± 0.25 µm; Supplementary Figure S4) and the dendrite from which it emerged was almost always the thickest basal dendrite at its initial portion (4.97 ± 0.27 µm compared to 1.98 ± 0.04 µm). The distance from the soma to the initiation of the axon within the dendrite was 12.10 ± 1.44 µm. In 4 pyramidal cells, the axons were of sufficient length (419.20 ± 75.26 µm) to include 1–4 axonal collaterals showing 70 axonal varicosities. Human axons gave off collaterals at a distance of 135.6 ± 38.4, 135.1 ± 7.5, 219.8 ± 43.5, and 267.2 ± 41.8 µm for the first, second, third, and fourth collaterals, respectively. The axonal varicosity density was 1.74 ± 0.23, 1.06 ± 0.02, 1.39 ± 0.08, and 1.31 ± 0.03 varicosities per 10 µm in the first, second, third, and fourth collaterals, respectively. The axonal intervaricosity distance was 6.53 ± 1.26, 3.45 ± 0.06, 3.75 ± 0.17, and 3.77 ± 0.68 µm in the first, second, third, and fourth collaterals, respectively.

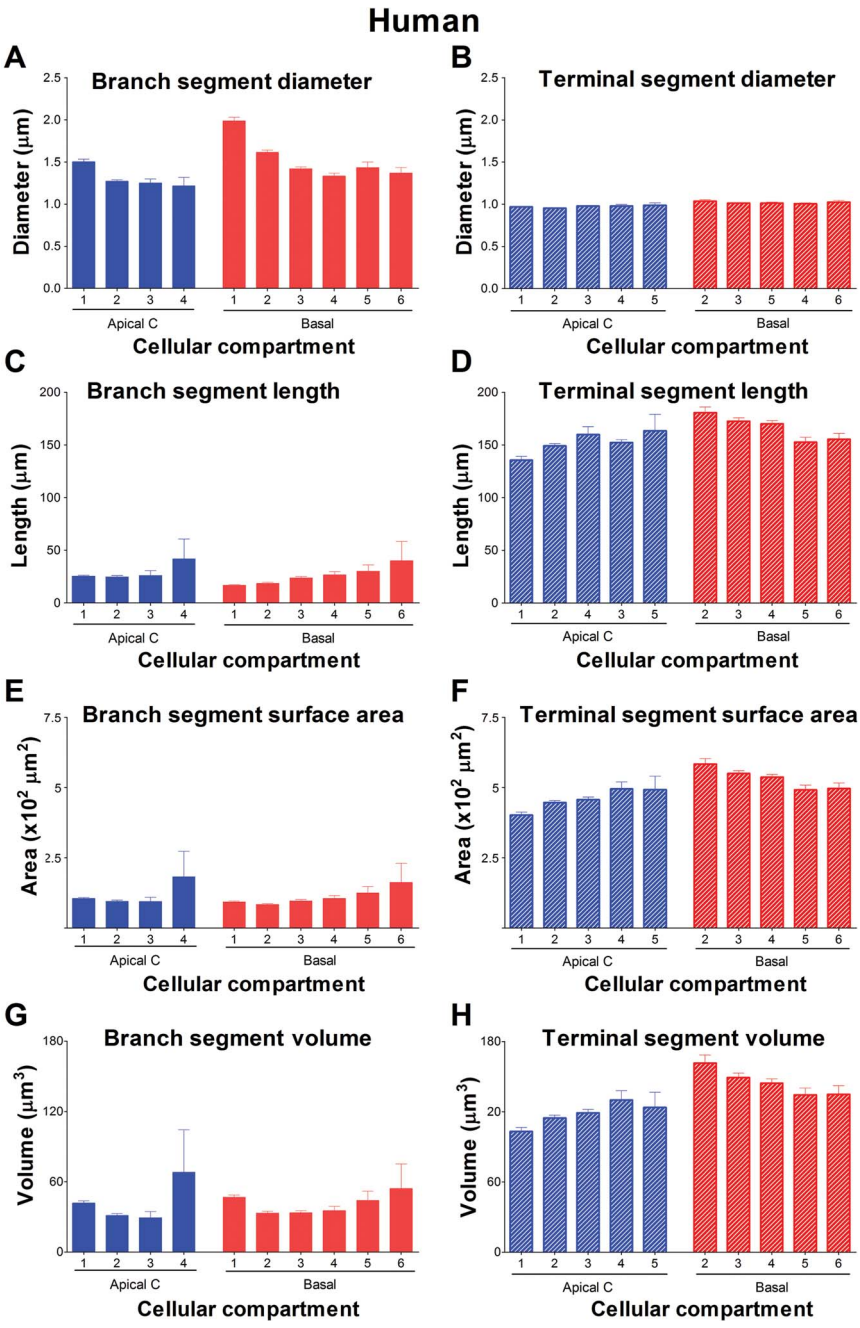

Figure 7. Graphs showing human branching (left column) and terminal (right column) dendritic segment diameter (*A* and *B*), segment length (*C* and *D*), segment surface area (*E* and *F*), and segment volume (*G* and *H*) for apical collateral dendrites (blue) and basal dendrites (red). Measurements are reported as mean ± SEM. Only dendritic segments that were complete, and thus excluding incomplete endings, were included in this analysis. Main apical dendrite was not included in the graph since no complete terminal segments were reconstructed for human neurons. Statistical significance of the differences is shown in Supplementary Tables 3 and 4.

Mouse CA1 Pyramidal Cells

Fifty mouse pyramidal cells were analyzed in the CA1 field. These cells presented a mean cell body area of 137 ± 3.0 µm^2.

Apical Dendrites

An apical arbor emerged from the soma and was composed of a prominent main apical dendritic shaft which gave off a number of oblique collaterals (14 to 31) during its ascending trajectory toward the pia mater. The extent of the apical shaft varied from 220–480 µm, including the apical tufts in most of the cases (~70%). The main apical shaft had the thickest and longest segments (Fig. 9A,D), whereas collateral dendrites had segments that were slightly thinner and longer than basal dendritic segments. The structure of the apical arbor as it emerged from the soma was mainly formed by a main apical dendrite that ran without branching to the beginning of the

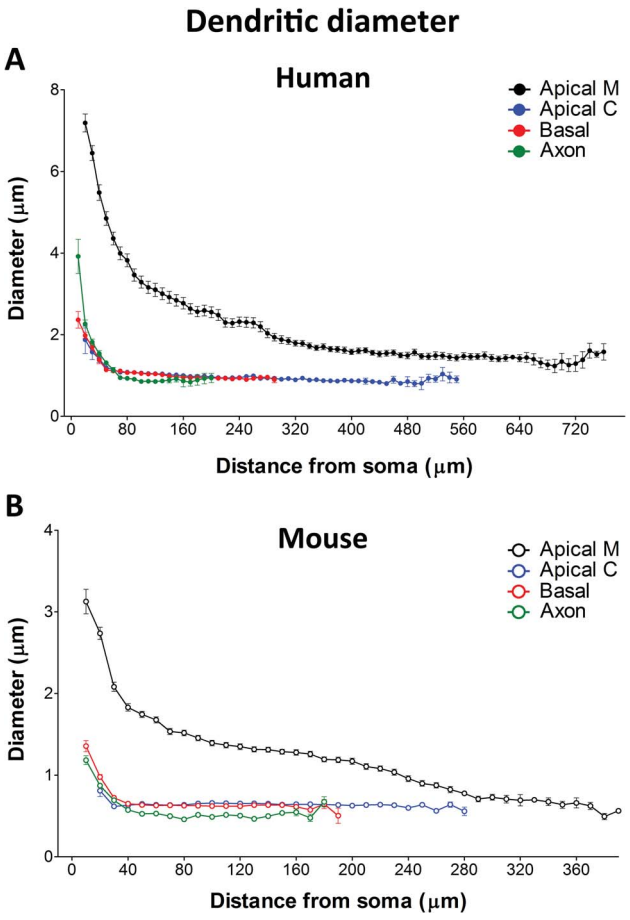

Figure 8. Graphs showing dendritic diameter distribution as a function of the distance from soma in human (A) and mouse (B) for main apical dendrites (black), collateral dendrites (blue), basal dendrites (red), and axon (green). Measurements are reported as mean ± SEM. Statistical significance of the differences is shown in Supplementary Tables 5 and 6. Please note that these graphs are not on the same scale. Human and mouse data comparison is shown in one graph in Fig. 13.

apical tuft, which appeared at a distance of 232.6 ± 4.33 µm from the cell body. However, 40% of them bifurcated once, whereas only one cell bifurcated twice and another one bifurcated three times before the beginning of the apical tuft. Thus, two main groups of cells were observed according to this feature: one without bifurcations and one with one bifurcation (Fig. 6 and Supplementary figure S5). The average diameter of the main apical shaft before any bifurcation occurred was 1.82 ± 0.05 µm. In the case that the apical dendrite branched before the apical tuft, the diameter decreased to 1.19 ± 0.04 µm (Fig. 9E). Apical tufts also decreased in diameter as branch order increased. The segment diameters of the same branching order were similar regardless of whether they belonged to the apical tuft or not. Regarding the length of branch segments, they decreased as branch order increased in the main apical dendrite but not in the apical tufts. Segments were shorter at the tuft (Fig. 9F). The surface area and volume of the branch dendritic segments also showed decreasing values in the main apical dendrite toward higher orders (Fig. 9G,H). The terminal segments of apical tufts (only acquired for branch orders 3 and 4) were thinner than branching segments (0.8 ± 0.02 and 0.6 ± 0.04 µm, respectively; Fig. 10A,B).

Collaterals of apical dendrites had an average diameter of 0.71 ± 0.01 µm as they emerged from the main apical dendrite up to the first node and slightly decreased in the following branch orders (Fig. 9E). The mean length of the dendritic segments remained quite similar in the different branch orders (Fig. 9F). Similarly, the surface area of the dendritic segments and their volume also remained similar in the different branch orders (Fig. 9G,H). When segments were classified according to branch and terminal segments, branch collateral segments followed a similar pattern of diameter distribution as described above, whereas terminal segments had similar diameters regardless of their branch order (Fig. 10A,B). Regarding the segment length, branch segments slightly increased while terminal segments decreased as branch order increased and were longer in terms of absolute values (Fig. 10C,D). Similarly, surface area and the volume of branch segments increased while terminal segments surface area and volume decreased toward higher orders and were larger in terms of absolute values (Fig. 10E–H).

Basal Dendrites

The basal dendritic arbor had 3.04 ± 0.16 primary basal branches with an average diameter of 1.19 ± 0.04 µm up to the first node, with the diameter decreasing somewhat to values that approximated 0.6 µm as the branch order increased (Fig. 9E). The mean length of the dendritic segments that composed the basal arbor increased as the branch order increased (Fig. 9F). Similarly, the surface area and volume of the dendritic segments also increased toward higher orders (Fig. 9G,H). When segments were classified according to their position within the arbor as branching segments or terminal segments, the branch segment diameter again decreased as branch order increased (Fig. 10A), while all terminal segments had a similar diameter regardless of the branch order they belonged to (Fig. 10B). Regarding the length and surface area, for short branching segments, they did not change as branch order segment increased but decreased for terminal segments (Fig. 10C-F). Volume of the dendritic segments decreased toward higher orders, both in branching and terminal segments (Fig. 10G,H).

When morphometric variables were measured according to the distance from the soma, the diameter gradually decreased from 3.12 ± 0.15 to ~0.6 µm along the length of the main apical dendrite (Fig. 8B); in the apical collateral dendrites the diameter decreased from 0.80 ± 0.07 to ~0. 6 µm along the first 30 µm and then remained similar at further distances (Fig. 8B). In the case of the basal dendrites, it decreased from 1.36 ± 0.07 to ~0.6 µm along the first 40 µm and then remained similar at further distances (Fig. 3E).

Additional Dendritic Features

Additional morphological dendritic non-full measurements including total values and measurements as a function of the distance from soma (Sholl analysis) are displayed in Supplementary figures S6 and S7. As the graphs shows the distribution of these parameters differs between main apical, apical collaterals, and basal arbors. For example, these measurements showed that the peak number of nodes in the basal arbor was located at ~30 µm and rapidly decreased (Supplementary Figure S7), which interestingly coincided with the location where basal dendritic diameter reached a constant value (~40 µm; Fig. 8B). However, similar to humans, in apical collateral dendrites, the distribution of nodes was different. The peak number of nodes was located at ~50 µm from the soma and

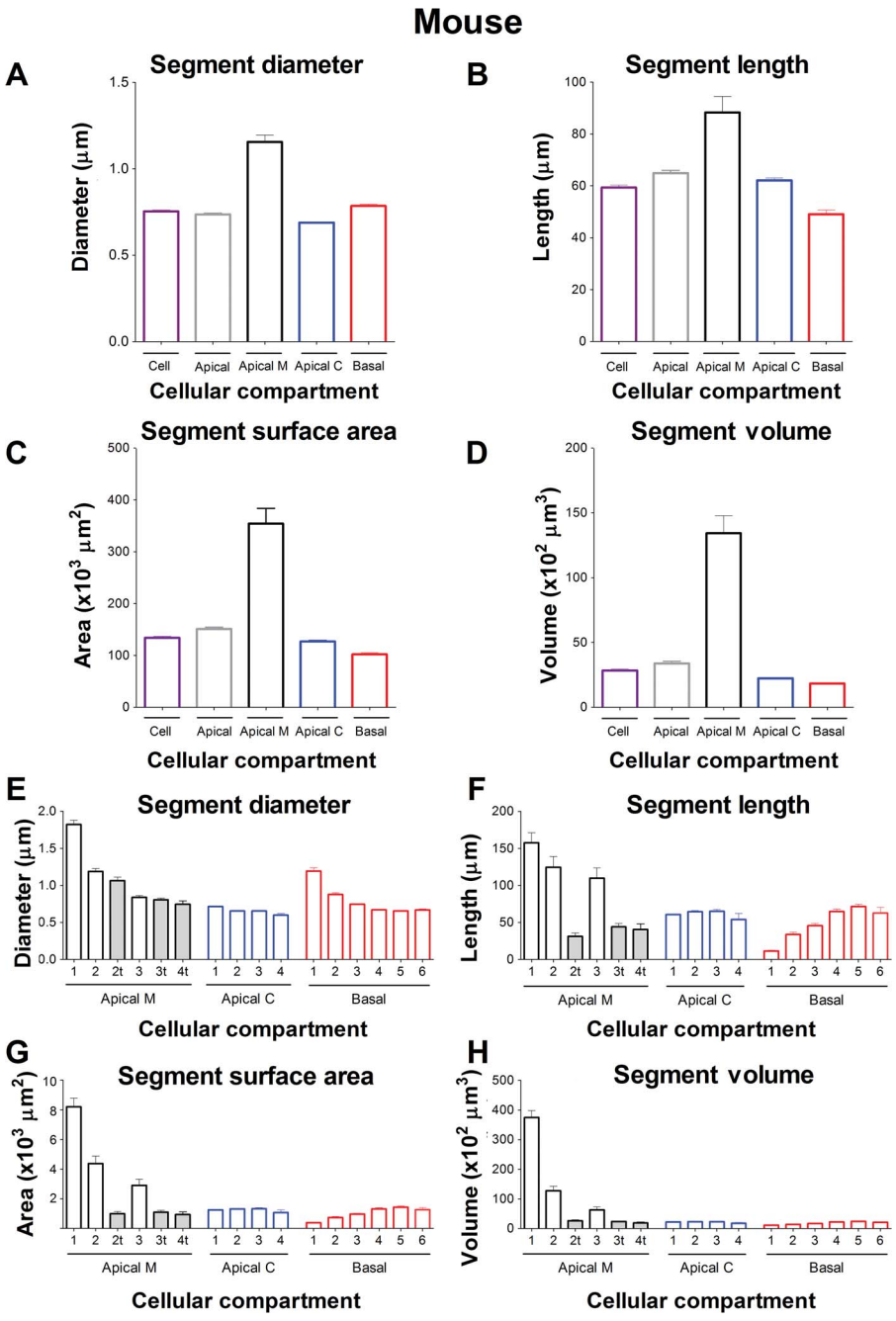

Figure 9. (*A–D*) Graphs showing mouse dendritic segment average diameter (*A*), segment length (*B*), segment surface area (*C*), and segment volume (*D*), expressed per cell (purple) and per dendritic compartment: apical arbor, including main apical dendritic shaft and apical collateral dendrites together (gray); main apical dendritic shaft only (black); apical collateral dendrites only (blue); and basal dendritic arbor (red). (*E–H*) Graphs showing same morphological variables as in (*A–D*): dendritic segment average diameter (*E*), segment length (*F*), segment surface area (*G*), and segment volume (*H*), expressed per branch order (1, 2, 3, etc.) and per dendritic compartment: main apical dendrite (black), apical collateral dendrites (blue), and basal arbor (red). Branch order segments in main apical dendrite are shown as belonging to the main apical shaft itself (1, 2, and 3) or belonging to the apical tuft (2t, 3t, and 4t). Measurements are reported as mean ± SEM. Only dendritic segments that were complete, and thus excluding incomplete endings, were included in this analysis. Statistical significance of the differences is shown in Supplementary Tables 7 and 8.

progressively decreased (Supplementary Figure S7), whereas the apical collateral dendritic diameter reached a constant value at ~30 µm (Fig. 8*B*).

Axon

The axons emerged mainly from the soma, although 20% of them emerged from the initial portion of a basal dendrite. The mean axonal diameter was 1.18 ± 0.05 µm and gradually decreased to ~0.5 µm along the first ~40 µm and then remained similar at further distances (Fig. 8*B*). In the cases that the axon emerged from the dendrite, its diameter was thinner (0.85 ± 0.23 µm; Supplementary Figure S4). Similar to our observations in human cells, the dendrite from which the axon emerged was found to be the thickest basal dendrite at

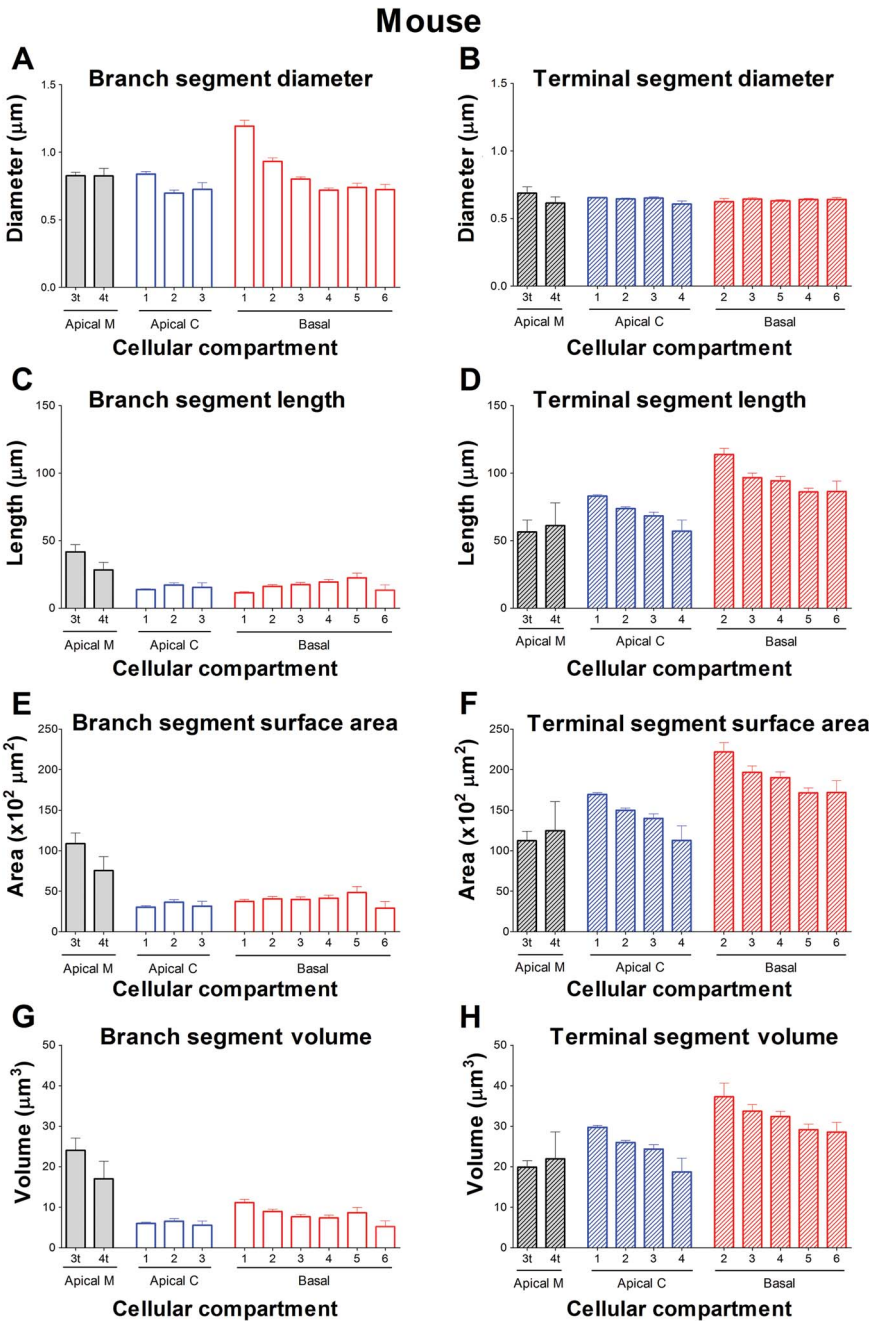

Figure 10. Graphs showing mouse branching (left column) and terminal (right column) dendritic segment diameter (*A* and *B*), segment length (*C* and *D*), segment surface area (*E* and *F*), and segment volume (*G* and *H*) for apical collateral dendrites (blue) and basal dendrites (red). Main apical dendrite includes values for the third and fourth tuft orders. No complete terminal segments were found for other orders. Measurements are reported as mean ± SEM. Only dendritic segments that were complete, and thus excluding incomplete endings, were included in this analysis. Main apical dendrite is included in the graph for the third and fourth tuft complete terminal segments, which were reconstructed for mouse neurons. Statistical significance of the differences is shown in Supplementary Tables 9 and 10.

its initial portion (2.4 ± 0.18 µm compared to 1.19 ± 0.04 µm mean dendritic thickness). The distance from the soma to the initiation of the axon arising from the dendrites was 3.75 ± 0.50 µm.

Human Versus Mouse Cell Comparisons

Human pyramidal cell bodies were larger (~350 µm²) compared to mouse (~140 µm²). Regarding the apical shaft, its length in the human varied from 230 to 800 µm (not including the apical tuft), whereas in the mouse it varied from 220 to 480 µm (including the apical tuft).

Mean values of dendritic segment diameter, length, surface area, and volume were much greater in the human than in the mouse (Fig. 11A,C,E,G). In both species, the main apical dendrite was the thickest, followed by the basal dendrites, and then the apical collateral dendrites. It should be noted that the human main apical shaft was much thicker than any other dendrite. In

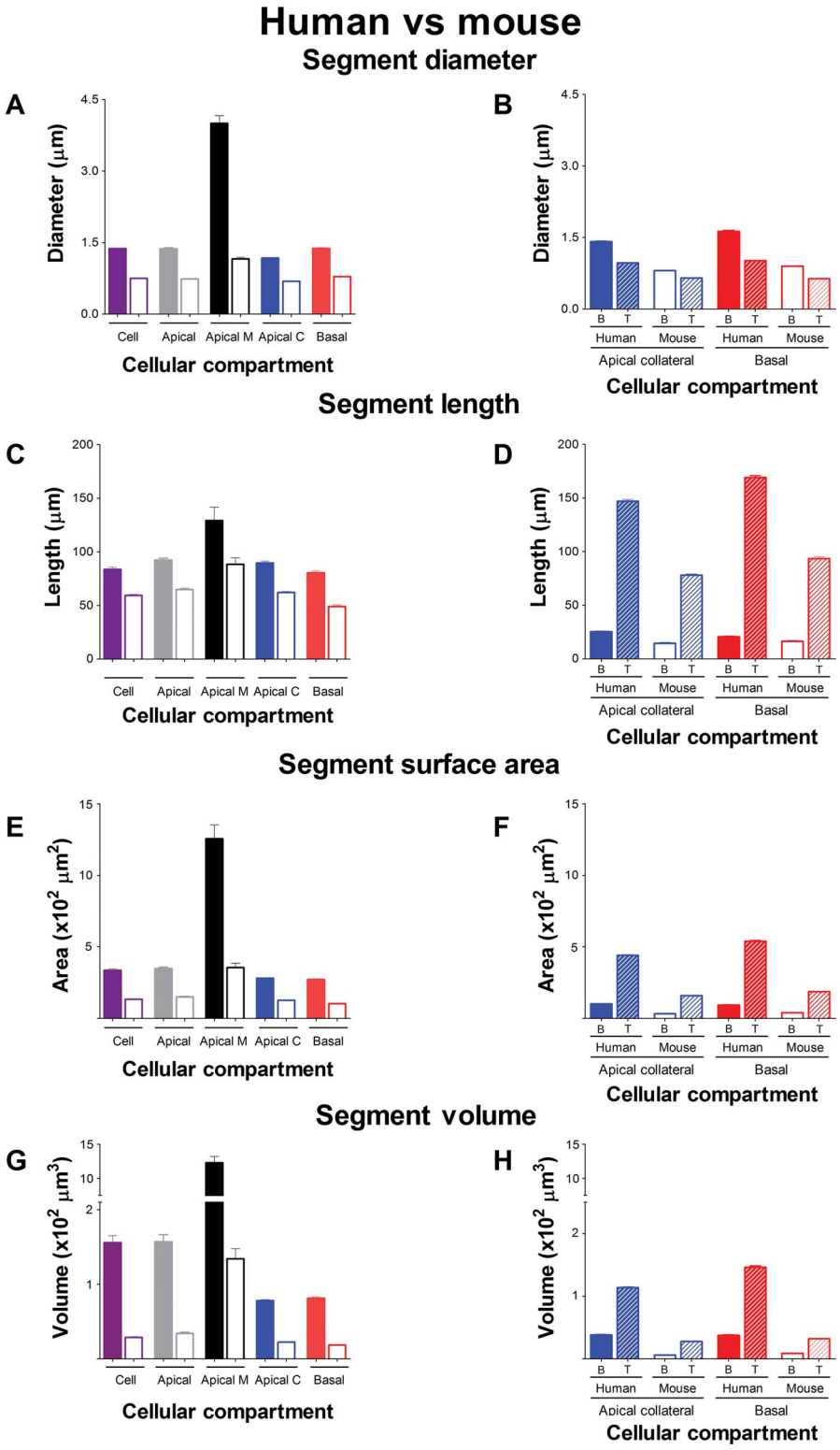

Figure 11. Left column: Graphs showing human versus mouse comparisons for dendritic segment average diameter (*A*), segment length (*C*), segment surface area (*E*), and segment volume (*G*), expressed per cell (purple) and per dendritic compartment: apical arbor, including main apical dendrite and apical collateral dendrites together (gray); main apical dendrite alone (black); apical collateral dendrites alone (blue); and basal dendritic arbor (red). Solid bars represent human neurons and outlined bars represent mouse neurons. Right column: Graphs showing human versus mouse comparisons of mean dendritic segment diameter (*B*), segment length (*D*), segment surface area (*F*), and segment volume (*H*), for apical collateral dendrites (blue) and basal dendrites (red), expressed per mean branching ("B") and terminal ("T") segments. Measurements are reported as mean ± SEM. Only dendritic segments that were complete, and thus excluding incomplete endings, were included in this analysis. Statistical significance of the differences is shown in Supplementary Tables 11 and 12.

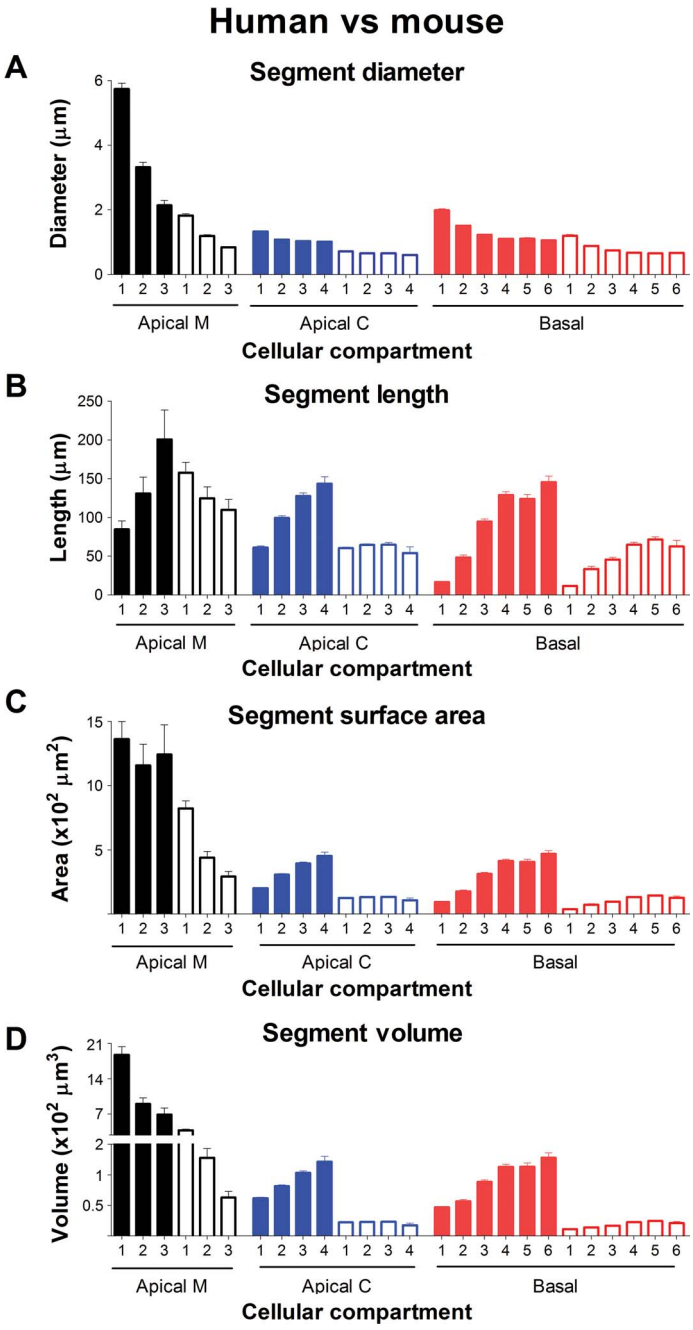

Figure 12. Graphs showing human and mouse comparisons for dendritic segment average diameter (*A*), segment length (*B*), segment surface area (*C*), and segment volume (*D*), expressed per branch order (1, 2, 3, etc.) and per dendritic compartment: main apical dendrite (black), apical collateral dendrites (blue) and basal arbor (red). Solid bars represent human neurons and outlined bars represent mouse neurons. Measurements are reported as mean ± SEM. Only dendritic segments that were complete, and thus excluding incomplete endings, were included in this analysis. Statistical significance of the differences is shown in Supplementary Table 13.

both species, the length of segments (between branch points) was the largest in apical dendrites, followed by the collateral apical dendrites, and the basal dendrites. This was also the case for surface area and volume in the mouse but not in the human, which showed similar values between compartments.

The structure of the apical arbor of the two species was different, showing a more complex structure with four main patterns of apical branching patterns compared to two main patterns in the mouse (Fig. 6). The average diameter of the main apical shaft before any bifurcation was thinner in the mouse (~2 µm) compared to the human (~5.5 µm; Fig. 12A). In both species, when the apical dendrite branched, the diameter decreased as the branch order increased (Fig. 12A). The length of dendritic segments increased as the branch order increased in the human,

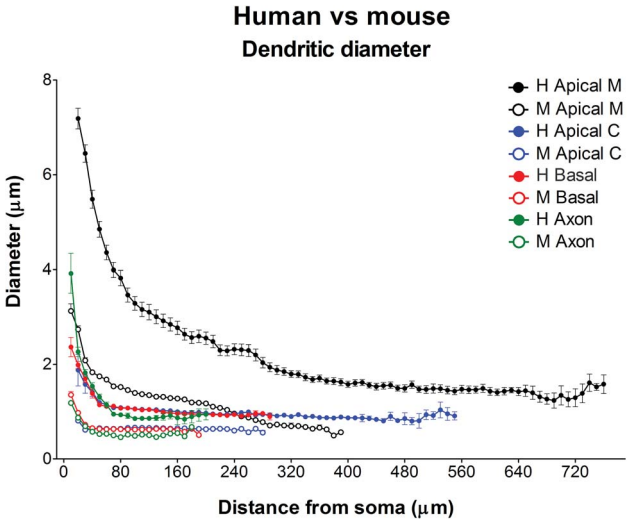

Figure 13. Graph showing human and mouse comparisons of dendritic diameter distribution as a function of the distance from soma in human (filled circles) and mouse (open circles) for main apical dendrites (black), collateral dendrites (blue), basal dendrites (red), and axon (green). Measurements are reported as mean ± SEM. Statistical significance of the differences is shown in Supplementary Table 14.

whereas it decreased as branch order increased in the mouse (Fig. 12B). As a consequence, the surface area of dendritic segments also showed a differential trend between the two species (Fig. 12C). The volume of main apical dendritic segments was much larger in the human compared to the mouse, although the trend of decreasing values toward higher orders was observed in both species (Fig. 12D).

Regarding collaterals of apical dendrites, primary branches showed an average diameter of ~1.33 in the human and ~0.7 µm in the mouse up to the first node and slightly decreased in the following branch orders in both species (Fig. 12A). The length of dendritic segments increased as the branch order increased in the human, whereas it remained relatively constant in the mouse (Fig. 12B). Thus, differential trends were also observed for surface area of the dendritic segments and their volume between the two species (Fig. 12C,D).

The primary dendrites of basal dendritic arbors had an average diameter of ~2 µm compared to ~1.2 µm in the mouse and slightly decreased in diameter as branch order increased in both species (Fig. 12A). The length of the dendritic segments that composed the basal arbors increased in both species as the branch order increased, although absolute values were smaller in the mouse (Fig. 12B). Similarly, the surface area and volume of the dendritic segments also increased toward higher orders, although the differences between orders were higher in the human (Fig. 12C,D).

When dendritic diameters were compared according to their distance from the soma, both the human and the mouse showed similar patterns of distribution of values in the different dendritic compartments, although absolute values of diameters differed greatly (Fig. 13): In the human main apical dendrite, the diameter decreased from ~7 to ~1.5 µm along the first 400 µm and remained similar at further distances, whereas in the mouse the diameter decreased from ~3 to ~0.6 µm along the length of the main apical dendrite. In the case of collateral apical dendrites, the diameters decreased from ~1.8 to ~1 µm along the first 50 µm in the human and from ~0.8 to ~0.6 µm along the first 30 µm in the mouse. Regarding the diameter of the human basal dendrites, it decreased from ~2 to ~1 µm along the first 60 µm, whereas in the mouse this diameter decreased from ~1.3 to ~0.6 µm along the first 40 µm but then remained similar at further distances in both species.

Axons emerged both from the soma (66%) and the initial portion of a basal dendrite (44%) in human, whereas in mouse ~20% of the axons were found to emerge from a basal dendrite. In humans, the axon emerging from the soma had a mean average diameter of 3.9 µm, whereas in the mouse this diameter was 1.17 µm. The axon diameter gradually decreased to 0.9 µm at a distance from the soma of 70 µm in the human, whereas in the mouse it decreased to ~0.5 µm along the first 40 µm (Fig. 13; Supplementary Figure S4). When the axon emerged from a dendrite, its diameter was found to be thinner (~1.8 µm in human; ~0.85 µm in mouse). In both species, the dendrite from which it emerged was found to be the thickest basal dendrite at its initial portion (~5 and ~2.4 µm in human and mouse, respectively). The distance from the soma to the initiation of the axon from the dendrite was ~12 µm in human and ~4 µm in mouse.

The comparison of measurements regarding the size (2D and 3D convex hulls), number of nodes, dendritic length, dendritic area, and dendritic volume expressed as total values are displayed in Figure 14, which shows that these variables were larger in most compartments of the human neurons. As a function of the distance from the soma, basal dendritic structure showed a higher peak complexity of nodes in humans, whereas collateral dendrites showed a similar maximum number of nodes between the species (Figs 15 and 16). The number of intersections, dendritic length, surface area, and volume, expressed as a function of the distance from the soma, was also larger in both apical and basal human dendrites compared to the mouse (Figs 15 and 16). See Table 1 for a summary comparing some measurements of the main variables.

Discussion

The main finding in the present study is that CA1 pyramidal neurons in the two species show characteristic cell morphologies. Human CA1 pyramidal neurons exhibit distinctive morphological complexity, which bears important computational implications. Human cells are not only larger but also have a structurally different organization compared to mouse cells regarding a number of morphometric features. However, there are some other morphological variables that have similar organizations in the two species although they do differ in their absolute values.

Differences Between Human and Mouse CA1 Pyramidal Cells

One obvious difference that often goes unnoticed is that, because of the corticalization of the human pyramidal cell layer of CA1, the connections must be different to those of rodents. Indeed, the stratum oriens is usually described in rodents as the layer occupied by basal dendrites of the pyramidal cells. Therefore, the excitatory connections with the basal dendrites are mostly restricted to this layer. Since the excitatory connections with the apical dendrites are restricted to the stratum radiatum and stratum lacunosum-moleculare, there is a clear stratification of excitatory connections in the rodent CA1. However, in the human CA1, basal dendrites and apical dendrites are mostly intermingled, meaning that the apical tree

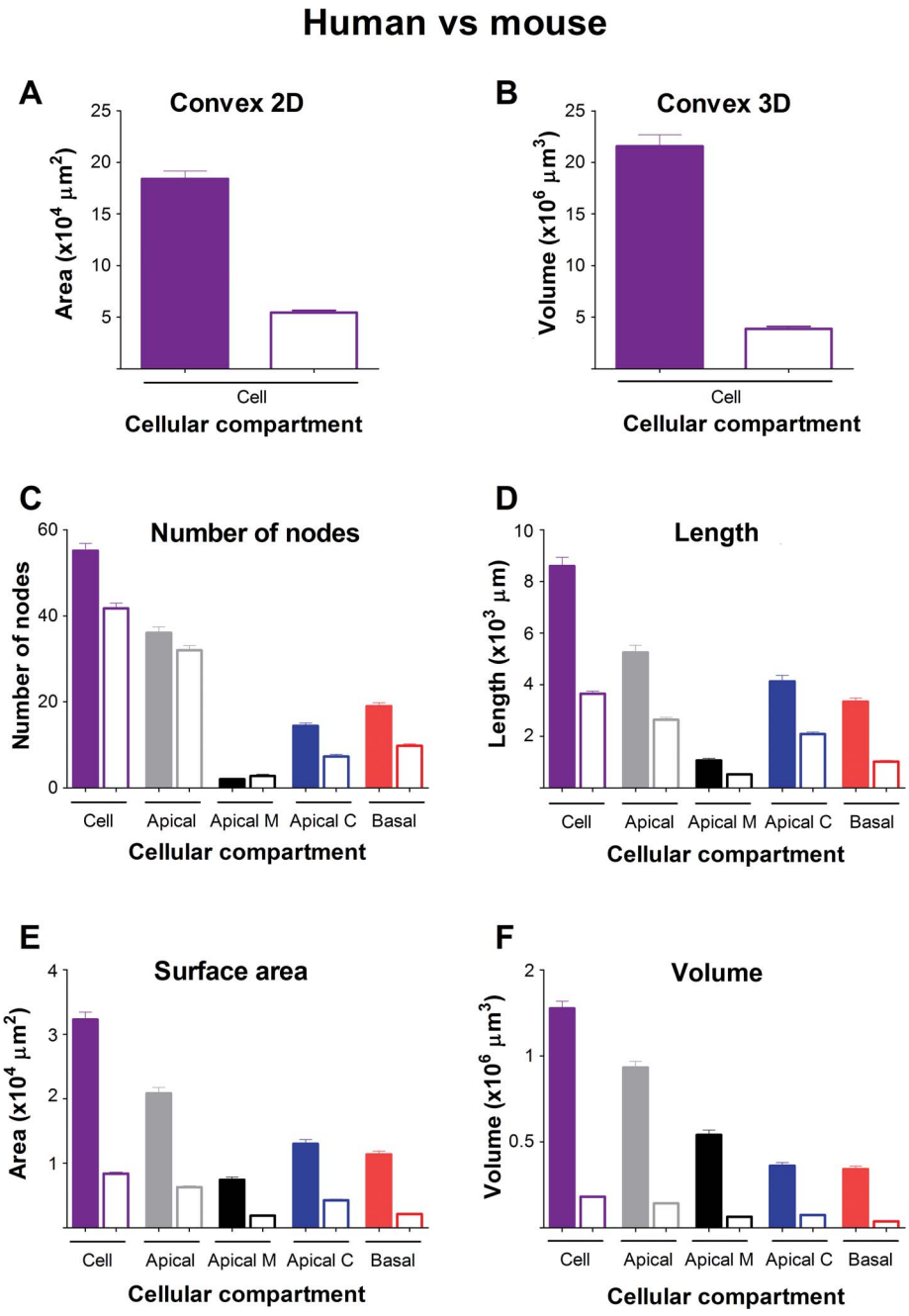

Figure 14. Graphs showing human and mouse comparisons of 2D (*A*) and 3D (*B*) convex hull, number of nodes (*C*), dendritic length (*D*), dendritic surface area (*E*), and dendritic volume (*F*), all expressed as total values, sorted by cell (purple) and by dendritic compartment: apical arbor, including main apical dendrite and apical collateral dendrites together (gray); main apical dendrite alone (black); apical collateral dendrites alone (blue); and basal dendritic arbor (red). Solid bars represent human neurons and outlined bars represent mouse neurons. Measurements are reported as mean ± SEM. Statistical significance of the differences is shown in Supplementary Table 15.

of one cell overlaps the basal tree of the other cell. Therefore, the excitatory inputs of the human pyramidal neurons do not follow this stratified pattern of connections. Certainly, these differences in the pattern of connections have a number of important functional consequences, although their significance has not yet been fully addressed.

Regarding pyramidal cell morphometry, in all compartments of the human neurons, the convex hull, dendritic length, dendritic area, and volume of cells were larger than in mouse. In terms of function, the size and extent of dendritic arbors relate to the sampling strategies of cells and mixing of inputs from multiple sources: cortical and subcortical afferents and local cortical excitatory and inhibitory inputs (e.g., Lund et al. 1993; Malach 1994; Elston et al. 1999; Elston 2003). Importantly, the extent of the differences was not always proportional between the two species. For example, soma size was 2.5 times bigger in

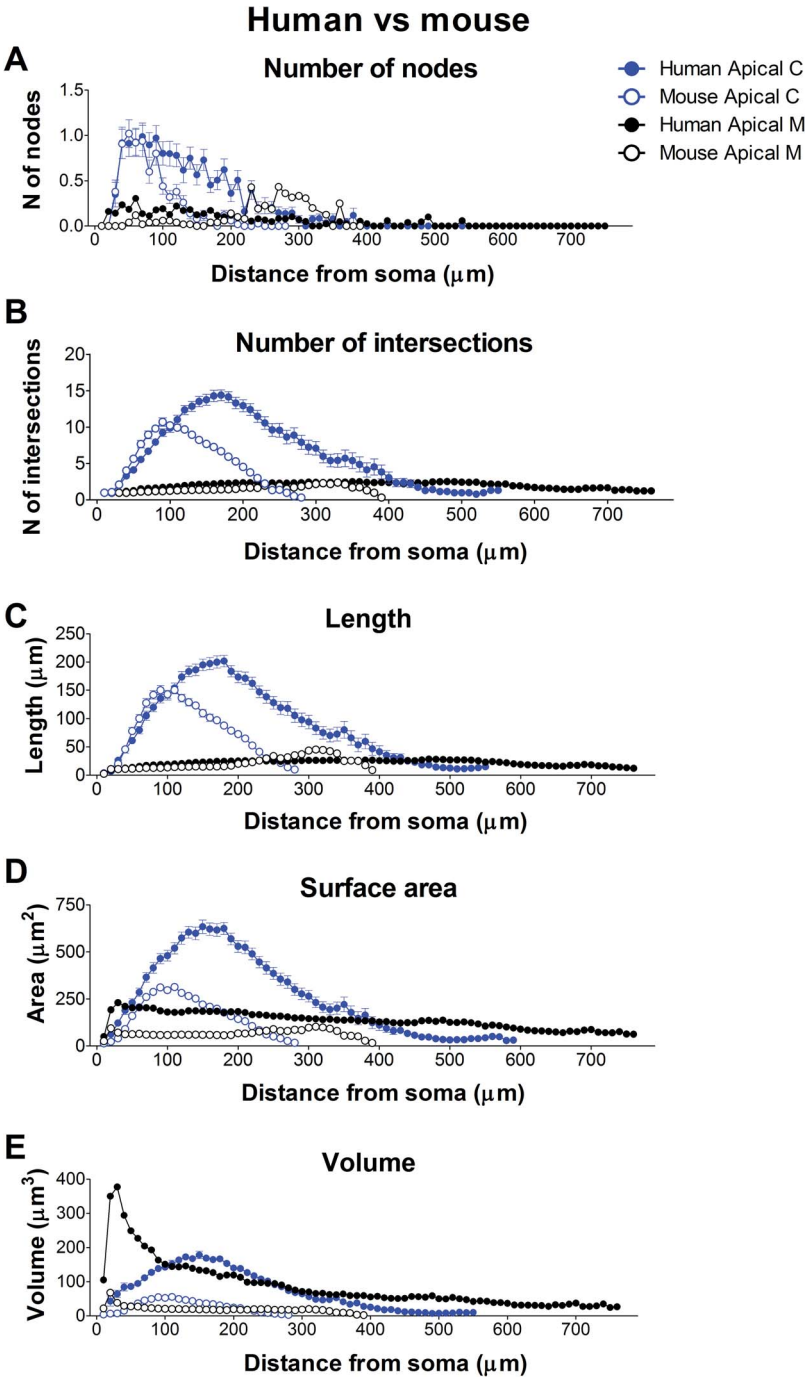

Figure 15. Graphs showing human and mouse comparisons of number of nodes (*A*), dendritic intersections (*B*), dendritic length (*C*), dendritic surface area (*D*), and dendritic volume (*E*) distribution as a function of the distance from soma in human (filled circles) and mouse (open circles) for main apical dendrites (black) and collateral dendrites (blue). Measurements are reported as mean ± SEM. Statistical significance of the differences is shown in Supplementary Table 16.

humans, whereas the basal extent was 1.5 times larger (Table 1). Thus, there is no linear scaling between the dendritic characteristics of human and mouse pyramidal cells analyzed in the present work.

It is worth noting that the differences found at the neuronal level between mice and human are ~2-fold, whereas the difference in the brain size between these two species is ~2800-fold (mouse brain volume = 0.5 cm^3; human brain volume = 1,400 cm^3; see e.g., Hofman, 2014). Indeed, biophysical constraints limit the size of neurons in all species, as the cable properties of the dendritic tree filter "dampens" the synaptic input that impinges on it. Consequently, dendrites are typically no more than ~2 space constants (λ) long. Otherwise, distal synapses would not have an impact on the cell's output (even in the nonlinear case; see recent work by Moldwin and Segev (2019) that specifically addresses the computational limitation on memo-

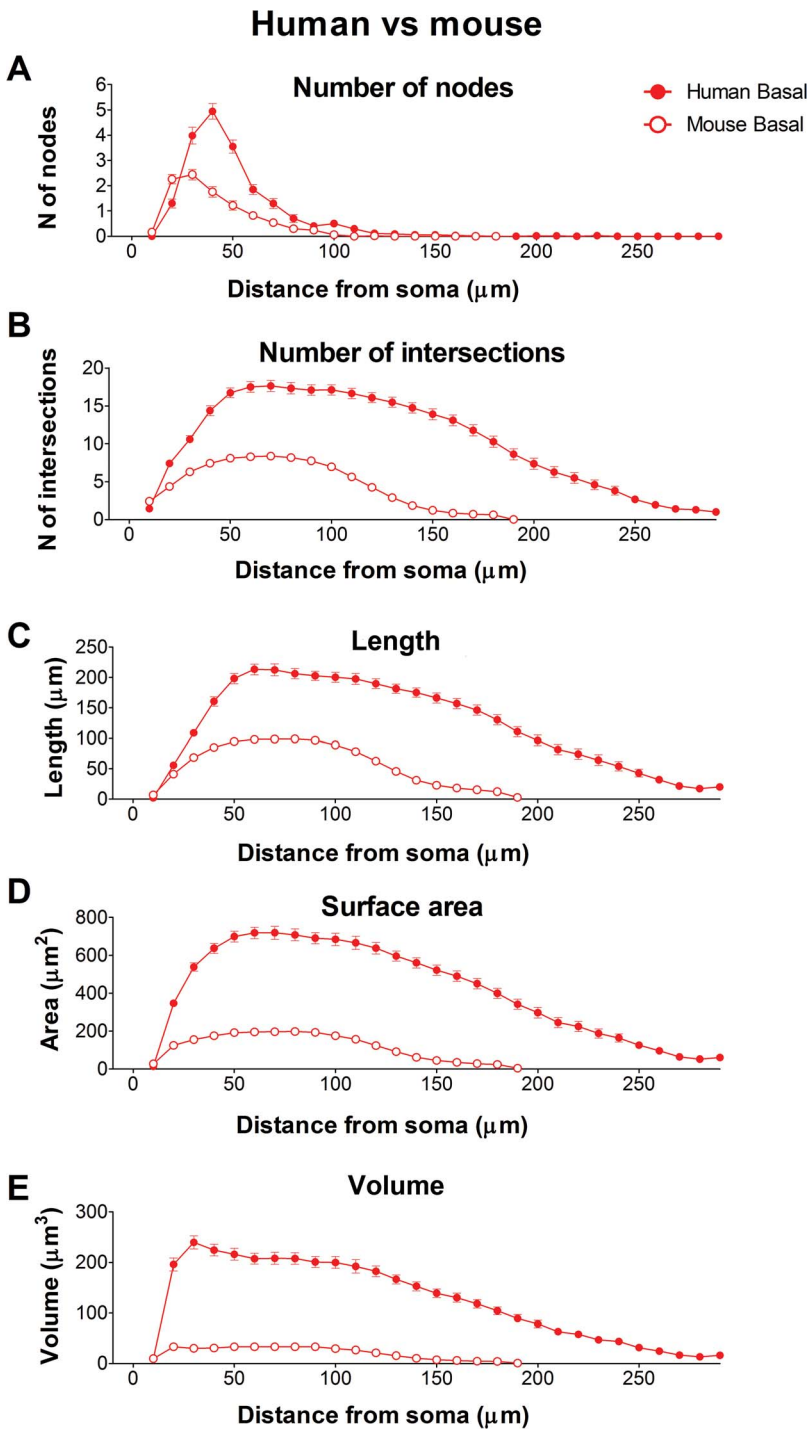

Figure 16. Graphs showing human and mouse comparisons of number of nodes (A), dendritic intersections (B), dendritic length (C), dendritic surface area (D) and dendritic volume (E) distribution as a function of the distance from soma in human (filled circles) and mouse (open circles) for basal dendrites. Measurements are reported as mean ± SEM. Statistical significance of the differences is shown in Supplementary table 16.

ry/generalization tasks due to the dendritic cable length). Additionally, the large dendritic trees of human cells had complex patterns of branching in the apical and basal dendrites that were not found in the mouse. In particular, several branching patterns were observed in the human main apical shaft compared to the mouse main apical shaft, which usually did not bifurcate or bifurcated once. In addition, there were about double the number of stem (primary) basal dendrites and also double the number of basal terminal endings in human versus mouse. Regarding the structure of apical arbors, previous studies have shown in the rat that pyramidal cells that can be distinguished by the morphology of their apical dendrites often have different

Table 1 Summary of some measurements (mean ± SEM) to illustrate the percentage increase of human values compared to mouse including soma size (estimated by measuring the area of the maximum perimeter of the soma), number of primary dendrites, basal extent (measured as the maximum concentric sphere centered on the cell body), distance from the soma of the maximum number of basal nodes (peak), average segment diameter of first- and second-order dendritic segment (in main apical shaft, apical collateral and basal), average segment length of first- and second-order dendritic segment (in main apical shaft, apical collateral and basal), average branching and terminal dendritic segment diameter (in apical collateral and basal), average branching and terminal dendritic segment length (in apical collateral and basal), average diameter at 10 µm Sholl distance (in main apical shaft, apical collateral, basal, axon emerging from soma, and axon emerging from dendrite), and average diameter of basal dendrites containing an emerging axon, for human and mouse.

	Human	Mouse	% Difference
Area of the maximum perimeter of the soma (μm^2)	350 ± 9.7	137 ± 3.0	255
Number of primary basal dendrites	6.37 ± 0.25	3.04 ± 0.15	209
Basal extent (μm)	300	190	158
Distance peak basal nodes (μm)	40	30	133
Segment diameter first-order main apical (μm)	5.74 ± 0.18	1.82 ± 0.05	302
Segment diameter second-order main apical (μm)	3.31 ± 0.15	1.19 ± 0.04	278
Segment diameter first-order apical collateral (μm)	1.33 ± 0.02	0.71 ± 0.01	187
Segment diameter second-order apical collateral (μm)	1.07 ± 0.01	0.65 ± 0.005	165
Segment diameter first-order basal (μm)	1.98 ± 0.04	1.19 ± 0.04	166
Segment diameter second-order basal (μm)	1.50 ± 0.02	0.88 ± 0.02	170
Segment length first-order main apical (μm)	84.77 ± 10.75	157.6 ± 13.54	54
Segment length second-order main apical (μm)	130.9 ± 21.08	124 ± 14.60	105
Segment length first-order apical collateral (μm)	60.99 ± 2.36	60.48 ± 1.33	101
Segment length second-order apical collateral (μm)	99.4 ± 2.94	64.54 ± 1.45	154
Segment length first-order basal (μm)	16.63 ± 0.80	11.48 ± 0.98	145
Segment length second-order basal (μm)	48.32 ± 3.28	33.64 ± 3.30	144
Segment branching diameter apical collateral (μm)	1.41 ± 0.02	0.81 ± 0.01	175
Segment terminal diameter apical collateral (μm)	0.96 ± 0.004	0.65 ± 0.002	148
Segment branching diameter basal (μm)	1.63 ± 0.01	0.90 ± 0.01	181
Segment terminal diameter basal (μm)	1.01 ± 0.005	0.64 ± 0.005	159
Segment branching length apical collateral (μm)	25.32 ± 0.80	14.57 ± 0.64	174
Segment terminal length apical collateral (μm)	147.1 ± 1.64	77.9 ± 0.78	188
Segment branching length basal (μm)	20.55 ± 0.66	16.43 ± 0.73	125
Segment terminal length basal (μm)	169.2 ± 1.78	93.51 ± 1.76	180
Average diameter at 10 μm Sholl main apical distance (μm)	7.19 ± 0.21	3.12 ± 0.15	230
Average diameter at 10 μm Sholl collateral distance (μm)	1.87 ± 0.33	0.80 ± 0.07	234
Average diameter at 10 μm Sholl basal distance (μm)	2.36 ± 0.20	1.36 ± 0.07	173
Average diameter at 10 μm Sholl axon distance emerging from soma (μm)	3.92 ± 0.42	1.18 ± 0.05	332
Average diameter at 10 μm Sholl axon distance emerging from dendrite (μm)	1.88 ± 0.25	0.85 ± 0.23	221
Average diameter of basal dendrites containing an emerging axon (μm)	4.97 ± 0.27	2.4 ± 0.18	207

firing patterns and seem to form distinct synaptic subnetworks (Wang et al. 2006; Feldmeyer 2012). Also, it has been shown in the rat somatosensory cortex that the morphological information of apical dendrites allows for a classification of pyramidal cells that largely corresponded to classes that were defined previously based on other neuronal and synaptic properties, such as long-range projects and synaptic innervations (Wang et al. 2018). Additionally, it has been shown in the rat hippocampus that neurons exhibiting different firing patterns have distinct physiological and morphological identities (Graves et al. 2012). Thus, it is likely that the various morphological types of branching patterns observed within and between the human and mouse give rise to different electrophysiological firing patterns.

In human pyramidal cells, the dendritic segments were thicker, longer, and had greater surface area and volume than in the mouse, in all compartments of the neuron. The human main apical dendrite was much thicker than any other dendrite, leading to a much larger surface area and volume than any other human dendrite. Furthermore, in the human, the length of segments in the main apical dendrite showed different trends as the branch order increased: It increased in the human, whereas it decreased in the mouse. Dendritic length of collateral segments increased as the branch order increased in the human, whereas it remained relatively constant in the mouse. Also, human terminal dendritic segments, both in basal and collateral dendrites, were larger than in mice and nonproportionally elongated (with respect to the nonterminal branches) when compared to the mouse. Altogether, these results show that human CA1 pyramidal cells are not a stretched version of mouse CA1 cells. Human cells have more complex dendritic tree and larger variable values that do not scale similarly between human and mouse. These differences in the geometrical design must reflect differences in cortical processing of information because the pattern of dendritic branching influences dendritic compartmentalization and, thus, the processing of information within their arbors (Rall 1959; Koch et al. 1982; Segev and London 2000; Poirazi and Mel 2001; London and Haüsser 2005; Spruston 2008; van Elburg and van Ooyen 2010 and see recent work on monkey V1 dendrites by Amatrudo et al. 2012 and by Luebke 2017, comparing mice and monkey dendritic topology).

Thus, the distinct properties observed in human and mouse pyramidal cells affect how they process information, enabling functional specialization of the neuronal networks in each species. Specifically in humans, the large and more complex structured pyramidal cells will allow for a greater capacity of the cells to perform a larger number of computations. These structural complexities potentially endow human CA1 neuron with multiple semi-independent, dendritic subunits. In this scenario, local synaptic inputs to a particular dendritic subtree may trigger there local nonlinearity (e.g., N-Methyl-D-aspartate [NMDA] spike) independent of such local nonlinearities in other dendritic subunits in the same CA1 neuron. Such multiple nonlinear subunits, enabled by the multitude dendritic branches in human CA1, are expected to enhance the computational/memory capacity of the neuron. Indeed, the connection between the increased morphological complexity in human versus mouse neurons and the enhanced computation capabilities in human neurons was recently demonstrated by Eyal et al. 2016 for human neocortical L2/3 pyramidal neurons (see also Gómez González et al. 2011; Beaulieu-Laroche et al. 2018). Also, the differential expression of ion channels between human and rodents has been shown to contribute to differences in neuronal physiology (Kalmbach et al. 2018). This is in line with recent work that has shown that larger dendritic trees enable pyramidal neurons to track activity of synaptic inputs with higher temporal precision, due to fast action potential kinetics (Goriounova et al. 2019).

Regarding axons, they were twice thicker in the human than in mouse and emerged both from the soma and the initial portion of a basal dendrite. In the mouse, the proportion of axons emerging from a basal dendrite was lower (see also Thome et al. 2014). In any case, the location of the origin of the axon is important since the spike initiation location may impact not only excitability but also the backpropagation of action potentials and synaptic integration (reviewed in Kole and Brette 2018). In this regard, the distance from the soma to the initiation of the axon in the dendrite was proportionally further away in humans—the axons emerged at a distance of around three-fourth of the length of the first-order dendrite compared to one-third in the case of the mouse. Taken together, these results show that differences between species are not only just in terms of size but also in the architecture of their cellular components, indicating that the structural designs of pyramidal cells in human and mouse are different.

Similarities in CA1 Pyramidal Cells Between Human and Mouse

Regarding similarities, there were several variables that differed in their absolute values but showed similar patterns of distribution between the two species. For example, in both species, the main apical shaft was the thickest, followed by the basal dendrites, and then the apical collateral dendrites. In the case that the apical dendrite branched, the diameter decreased as the branch order increased. In both species, differences in thickness between basal and collateral dendrites were mainly due to the larger diameter of the first- and second-order basal dendrites, whereas terminal segments were of the same thickness regardless of their branch order, both in collateral and basal dendrites. In both species, apical dendrites had the largest segments, followed by collateral dendrites, and then basal dendrites. Nodes were located close to the soma, at the same proportional distance (13–15%) from the extent of the basal dendrites. The maximum branching complexity of basal dendrites was higher and closer to the soma than that of collateral dendrites. The length of segments that branched was much smaller than that of terminal segments, both in collateral and basal dendrites. Also, in both species the terminal segments in the basal dendrites were longer than those of the collateral dendrites. Some of these similarities have also been observed in other species and cortical areas. For example, in the visual cortex of the rat (Larkman 1991), it was also shown that most basal dendritic branching occurred close to the soma, such that terminal segments were much longer than intermediate segments; terminal segments showed only a narrow range of diameters; collateral dendrites tended to be less highly branched but were otherwise extremely similar to basal trees; and the terminal segments tended to be thinner than those of basal or proximal oblique trees. In Bannister and Larkman (1995) the analysis of dendritic branching patterns of pyramidal neurons in the CA1 field of the rat, similar to observations in the present work, showed that the majority of branch points occurred close to the origin of the tree, and both basal and oblique terminal segments were generally much longer than intermediate segments. However, they observed that basal and oblique trees had similar branching patterns, which was not the case for the mouse and human CA1 cells, nor for the rat visual cortex (see above).

Regarding the axon, in the case that it emerged from the dendrite, its diameter was thinner in both species. Also, the dendrite from which it emerged was the thickest basal dendrite at its initial portion (~5 and ~2.4 µm thick, in human and mouse, respectively). These results suggest that there are some morphological parameters of the pyramidal cells that are conserved across species. Importantly, there is a functional segregation of CA1 pyramidal cells along the longitudinal axis—dorsoventral in rodents and anteroposterior in primates—and the proximodistal axis—proximal and distal are portions of CA1 that are adjacent to CA2 and subiculum, respectively (Igarashi et al. 2014; Strange et al. 2014; Soltesz and Losonczy 2018). Further studies along these axes and in other cortical regions and species would be necessary to elucidate which of these similarities might be considered as basic elements of the design of pyramidal cells and which are adaptations to particular regions. Finally, since the dendritic spines of pyramidal cells are key dendritic elements that contribute actively to the integration of information and synaptic plasticity (Hausser et al. 2000; Anderson et al. 2007; Harvey and Svoboda 2007; Spruston 2008; Yuste 2010), future studies on the density, distribution, and morphology of dendritic spines are necessary to further understand the processing of these cells within neuronal circuits. Also, the number of semi-independent dendritic subunits depend on the degree of electrical decoupling between dendritic subunits (Eyal et al. 2018), and these depend on the specific axial and membrane resistivity and on the membrane capacitance, as well as on the diameter of the respective dendritic branches. Further physiological studies on CA1 neurons would enable to obtain the cable parameters of human CA1 neurons and, consequently, to study via detailed cable models, if indeed the number of functional nonlinear dendritic subtrees is large in human CA1 neurons, as is strongly indicated by their highly complex dendritic tree.

Methodological Considerations

The mice used in the study are still relatively young at 8 weeks, whereas we used two middle-aged human cases (45 and 53 years). Thus, it is possible that age may have an

effect on some of the dendritic parameters assessed (see Benavides-Piccione et al. 2013 and references contained therein). Nevertheless, the differences between the mouse and human neurons are so large that most likely these differences represent species-specific differences rather than age-related differences. Indeed, Jacobs et al. (1997) studied the pyramidal cell structure of neurologically normal individuals ranging in age from 14 to 106 years using the Golgi method. They found that dendritic values were relatively stable after 40 years of age. Another possible limitation when comparing mice and human neurons is that human brain has been fixed by immersion, whereas mouse brains have been fixed by intracardial perfusion. However, as previously discussed (Benavides-Piccione et al. 2002), we did not find any obvious difference between the two methods of fixation.

Furthermore, since 3D reconstructions do not include complete basal and apical arbors (see Materials and Methods for further details), results from variables that do depend on the entirety of the cell (2D and 3D convex hulls, total number of dendrites, nodes, intersections, total dendritic length, surface area, and volume) should be interpreted with these technical limitations on mind. On the contrary, morphological variables that do not depend on the entirety of the reconstructed cell (soma area, segment diameter, segment length, segment surface area, and segment volume) do not have these restrictions and these measurements can be reliably compared. Finally, although we reconstructed a relatively large number of reconstructed human pyramidal cells ($n = 54$), they came from only two individuals. This limited number of cases was due to the difficulties in obtaining human tissue with the optimal quality of fixation required for these experiments. Nevertheless, the results obtained in the present study are robust due to the large number of dendritic morphological characteristics that were analyzed. In addition, there are no other similar studies performed in the normal human hippocampus. Thus, the present study represents a further step toward the characterization of human brain microorganization, although it would be necessary to confirm with a larger number of individuals.

Supplementary Material

Supplementary material is available at *Cerebral Cortex* online.

Notes

We would like to thank Debora Cano, Lorena Valdes, Carmen Alvarez, Miriam Marin, and Ana García for technical assistance.

Funding

Spanish "Ministerio de Ciencia, Innovación y Universidades" (grant SAF 2015-66603-P and the Cajal Blue Brain Project [C080020-09; the Spanish partner of the Blue Brain Project initiative from L'Ecole polytechnique fédérale de Lausanne (EPFL), Switzerland]); European Union's Horizon 2020 Research and Innovation Programme (grant 785907) (Human Brain Project second specific grant agreement [SGA2]).

References

Amatrudo JM, Weaver CM, Crimins JL, Hof PR, Rosene DL, Luebke JI. 2012. Influence of highly distinctive structural properties on the excitability of pyramidal neurons in monkey visual and prefrontal cortices. *J Neurosci*. 32:13644–13660.

Anderson P, Morris R, Amaral DG, Bliss T, O'Keefe J. 2007. *The hippocampus book*. Oxford (UK): OUP.

Ballesteros-Yáñez I, Benavides-Piccione R, Bourgeois JP, Changeux JP, DeFelipe J. 2010. Alterations of cortical pyramidal neurons in mice lacking high-affinity nicotinic receptors. *Proc Natl Acad Sci U S A*. 107:11567–11572.

Bannister NJ, Larkman AU. 1995. Dendritic morphology of CA1 pyramidal neurones from the rat hippocampus: I. branching patterns. *J Comp Neurol*. 360:150–160.

Beaulieu-Laroche L, Toloza EHS, van der Goes MS, Lafourcade M, Barnagian D, Williams ZM, Eskandar EN, Frosch MP, Cash SS, Harnett MT. 2018. Enhanced dendritic compartmentalization in human cortical neurons. *Cell*. 175:643–651.

Benavides-Piccione R, Ballesteros-Yáñez I, Defelipe J, Yuste R. 2002. Cortical area and species differences in dendritic spine morphology. *J Neurocytol*. 31:337–346.

Benavides-Piccione R, Fernaud-Espinosa I, Robles V, Yuste R, DeFelipe J. 2013. Age-based comparison of human dendritic spine structure using complete three-dimensional reconstructions. *Cereb Cortex*. 23:1798–1810.

Benavides-Piccione R, Hamzei-Sichani F, Ballesteros-Yáñez I, DeFelipe J, Yuste R. 2006. Dendritic size of pyramidal neurons differs among mouse cortical regions. *Cereb Cortex*. 16:990–1001.

Bianchi S, Stimpson CD, Bauernfeind AL, Schapiro SJ, Baze WB, McArthur MJ, Bronson E, Hopkins WD, Semendeferi K, Jacobs B *et al*. 2013. Dendritic morphology of pyramidal neurons in the chimpanzee neocortex: regional specializations and comparison to humans. *Cereb Cortex*. 23:2429–2436.

Cenquizca LA, Swanson LW. 2007. Spatial organization of direct hippocampal field CA1 axonal projections to the rest of the cerebral cortex. *Brain Res Rev*. 56:1–26.

DeFelipe J. 2011. The evolution of the brain, the human nature of cortical circuits and intellectual creativity. *Front Neuroanat*. 5:29.

DeFelipe J, Fariñas I. 1992. The pyramidal neuron of the cerebral cortex: morphological and chemical characteristics of the synaptic inputs. *Prog Neurobiol*. 39:563–607 (review).

Deitcher Y, G E, Kanari L, Verhoog MB, Atenekeng Kahou GA, Mansvelder HD, de Kock CPJ, Segev I. 2017. Comprehensive morpho-electrotonic analysis shows 2 distinct classes of L2 and L3 pyramidal neurons in human temporal cortex. *Cereb Cortex*. 27:5398–5414.

Domínguez-Álvaro M, Montero-Crespo M, Blazquez-Llorca L, Insausti R, DeFelipe J, Alonso-Nanclares L. 2018. Three-dimensional analysis of synapses in the transentorhinal cortex of Alzheimer's disease patients. *Acta Neuropathol Commun*. 6:20.

Elston GN. 2003. Cortex, cognition and the cell: new insights into the pyramidal neuron and prefrontal function. *Cereb Cortex*. 13:1124–1138.

Elston GN, Arellano J, González-Albo MC, DeFelipe J, Rosa MG. 1999. Variation in the spatial relationship of parvalbumin immunoreactive interneurones and pyramidal neurones in the somatosensory cortex of the rat. *Neuroreport*. 10:2975–2979.

Elston GN, Benavides-Piccione R, DeFelipe J. 2001. The pyramidal cell in cognition: a comparative study in human and monkey. *J. Neurosci*. 21:RC163.

Eyal G, Verhoog MB, Testa-Silva G, Deitcher Y, Benavides-Piccione R, DeFelipe J, de Kock CPJ, Mansvelder HD, Segev I. 2018. Human cortical pyramidal neurons: from spines to spikes via models. *Front Cell Neurosci*. 12:181.

Eyal G, Verhoog MB, Testa-Silva G, Deitcher Y, Lodder JC, Benavides-Piccione R, Morales J, DeFelipe J, de Kock CP, Mansvelder HD *et al*. 2016. Unique membrane properties and enhanced signal processing in human neocortical neurons. *Elife*. 5:e16553.

Feldmeyer D. 2012. Excitatory neuronal connectivity in the barrel cortex. *Front Neuroanat*. 6:24.

Gómez González JF, Mel BW, Poirazi P. 2011. Distinguishing linear vs. non-linear integration in CA1 radial oblique dendrites: it's about time. *Front Comput Neurosci*. 5:44.

Goriounova NA, Heyer DB, Wilbers R, Verhoog MB, Giugliano M, Verbist C, Obermayer J, Kerkhofs A, Smeding H, Verberne M *et al*. 2019. Large and fast human pyramidal neurons associate with intelligence. *Elife*. 7:e41714.

Graves AR, Moore SJ, Bloss EB, Mensh BD, Kath WL, Spruston N. 2012. Hippocampal pyramidal neurons comprise two distinct cell types that are countermodulated by metabotropic receptors. *Neuron*. 76:776–789.

Harvey CD, Svoboda K. 2007. Locally dynamic synaptic learning rules in pyramidal neuron dendrites. *Nature*. 450: 1195–1200.

Hausser M, Spruston N, Stuart GJ. 2000. Diversity and dynamics of dendritic signaling. *Science*. 290:739–744.

Hofman MA. 2014. Evolution of the human brain: when bigger is better. *Front Neuroanat*. 8:15 doi: 10.3389/fnana.2014.00015.

Igarashi KM, Ito HT, Moser EI, Moser MB. 2014. Functional diversity along the transverse axis of hippocampal area CA1. *FEBS Lett*. 588:2470–2476.

Insausti R, Amaral DG. 2012. Hippocampal formation. In: Mai JK, Paxinos G, editors. *The human nervous system*. 3rd ed. San Diego (CA): Academic Press.

Jacobs B, Driscoll L, Schall M. 1997. Life-span dendritic and spine changes in areas 10 and 18 of human cortex: a quantitative Golgi study. *J Comp Neurol*. 386:661–680.

Jacobs B, Schall M, Prather M, Kapler E, Driscoll L, Baca S, Jacobs J, Ford K, Wainwright M, Treml M. 2001. Regional dendritic and spine variation in human cerebral cortex: a quantitative study. *Cereb Cortex*. 11:558–571.

Jarsky T, Mady R, Kennedy B, Spruston N. 2008. Distribution of bursting neurons in the CA1 region and the subiculum of the rat hippocampus. *J Comp Neurol*. 506:535–547.

Kalmbach BE, Buchin A, Long B, Close J, Nandi A, Miller JA, Bakken TE, Hodge RD, Chong P, de Frates R *et al*. 2018. H-channels contribute to divergent intrinsic membrane properties of supragranular pyramidal neurons in human versus mouse cerebral cortex. *Neuron*. 100:1194–1208.

Koch C, Poggio T, Torre V. 1982. Retinal ganglion cells: a functional interpretation of dendritic morphology. *Philos Trans R Soc Lond B Biol Sci*. 298:227–264.

Kole MH, Brette R. 2018. The electrical significance of axon location diversity. *Curr Opin Neurobiol*. 51:52–59.

Krimer LS, Jakab RL, Goldman-Rakic PS. 1997. Quantitative three-dimensional analysis of the catecholaminergic innervation of identified neurons in the macaque prefrontal cortex. *J Neurosci*. 17:7450–7461.

Larkman AU. 1991. Dendritic morphology of pyramidal neurones of the visual cortex of the rat: I. branching patterns. *J Comp Neurol*. 306:307–319.

Lee SH, Marchionni I, Bezaire M, Varga C, Danielson N, Lovett-Barron M, Losonczy A, Soltesz I. 2014. Parvalbumin-positive basket cells differentiate among hippocampal pyramidal cells. *Neuron*. 82:1129–1144.

London M, Häusser M. 2005. Dendritic computation. *Annu Rev Neurosci*. 28:503–532.

Luebke JI. 2017. Pyramidal neurons are not generalizable building blocks of cortical networks. *Front Neuroanat*. 11:11.

Lund JS, Yoshioka T, Levitt JB. 1993. Comparison of intrinsic connectivity in different areas of macaque monkey cerebral cortex. *Cereb Cortex*. 3:148–162.

Malach R. 1994. Cortical columns as devices for maximizing neuronal diversity. *Trends Neurosci*. 17:101–104.

Mohan H, Verhoog MB, Doreswamy KK, Eyal G, Aardse R, Lodder BN, Goriounova NA, Asamoah B, B Brakspear AB, Groot C *et al*. 2015. Dendritic and Axonal Architecture of Individual Pyramidal Neurons across Layers of Adult Human Neocortex. *Cereb Cortex*. 25:4839–4853.

Moldwin T, Segev I. 2019. Perceptron learning and classification in a modeled cortical pyramidal cell. bioRxiv 464826. doi: https://doi.org/10.1101/464826

Patzke N, Olaleye O, Haagensen M, Hof PR, Ihunwo AO, Manger PR. 2013. Organization and chemical neuroanatomy of the African elephant (Loxodonta africana) hippocampus. *Brain Struct Funct*. 219:1587–1601.

Paxinos G, Franklin KBJ. 2004. *The mouse brain in stereotaxic coordinates*. San Diego (CA): Elsevier.

Poirazi P, Mel BW. 2001. Impact of active dendrites and structural plasticity on the memory capacity of neural tissue. *Neuron*. 29:779–796.

Rall W. 1959. Branching dendritic trees and motoneuron membrane resistivity. *Exp Neurol*. 1:491–527.

Rojo C, Leguey I, Kastanauskaite A, Bielza C, Larrañaga P, DeFelipe J, Benavides-Piccione R. 2016. Laminar Differences in Dendritic Structure of Pyramidal Neurons in the Juvenile Rat Somatosensory Cortex. *Cereb Cortex*. 26: 2811–2822.

Segev I, London M. 2000. Untangling dendrites with quantitative models. *Science*. 290:744–750 (review).

Slomianka L, Amrein I, Knuesel I, Sørensen JC, Wolfer DP. 2011. Hippocampal pyramidal cells: the reemergence of cortical lamination. *Brain Struct Funct*. 216:301–317.

Soltesz I, Losonczy A. 2018. CA1 pyramidal cell diversity enabling parallel information processing in the hippocampus. *Nat Neurosci*. 21:484–493.

Spruston N. 2008. Pyramidal neurons: dendritic structure and synaptic integration. *Nat Rev Neurosci*. 9:206–221.

Stephan H, Andy OJ. 1970. The allocortex in primates. In: Noback CR, Montagna W, editors. *The primate brain*. New York: Appleton Century Crofts.

Strange BA, Witter MP, Lein ES, Moser EI. 2014. Functional organization of the hippocampal longitudinal axis. *Nat Rev Neurosci*. 15:655–669.

Stuart GJ, Spruston N. 2015. Dendritic integration: 60 years of progress. *Nat Neurosci*. 18:1713–1721.

Thome C, Kelly T, Yanez A, Schultz C, Engelhardt M, Cambridge SB, Both M, Draguhn A, Beck H, Egorov AV. 2014. Axon-carrying dendrites convey privileged synaptic input in hippocampal neurons. *Neuron*. 83: 1418–1430.

Valero M, de la Prida LM. 2018. The hippocampus in depth: a sublayer-specific perspective of entorhinal–hippocampal function. *Curr Opin Neurobiol*. 52:107–114.

Van Aerde KI, Feldmeyer D. 2015. Morphological and physiological characterization of pyramidal neuron subtypes in rat medial prefrontal cortex. *Cereb Cortex*. 25:788–805.

Van Elburg RA, Van Ooyen A. 2010. Impact of dendritic size and dendritic topology on burst firing in pyramidal cells. *PLoS Comput Biol*. 6:e1000781.

Wang Y, Markram H, Goodman PH, Berger TK, Ma J, Goldman-Rakic PS. 2006. Heterogeneity in the pyramidal network of the medial prefrontal cortex. *Nat Neurosci*. 9: 534–542.

Wang Y, Ye M, Kuang X, Li Y, Hu S. 2018. A simplified morphological classification scheme for pyramidal cells in six layers of primary somatosensory cortex of juvenile rats. *IBRO Rep*. 5:74–90.

Yuste R. 2010. *Dendritic spines*. Cambridge (MA): MIT Press.